

Multilevel quasi Monte Carlo methods for elliptic PDEs with random field coefficients via fast white noise sampling*

M. Croci^{††}M. B. Giles[†]P. E. Farrell[†]

November 28, 2019

Abstract

When solving partial differential equations with random fields as coefficients the efficient sampling of random field realisations can be challenging. In this paper we focus on the fast sampling of Gaussian fields using quasi-random points in a finite element and multilevel quasi Monte Carlo (MLQMC) setting. Our method uses the SPDE approach combined with a new fast (ML)QMC algorithm for white noise sampling. We express white noise as a wavelet series expansion that we divide in two parts. The first part is sampled using quasi-random points and contains a finite number of terms in order of decaying importance to ensure good QMC convergence. The second part is a correction term which is sampled using standard pseudo-random numbers. We show how the sampling of both terms can be performed in linear time and memory complexity in the number of mesh cells via a supermesh construction, yielding an overall linear cost. Furthermore, our technique can be used to enforce the MLQMC coupling even in the case of non-nested mesh hierarchies. We demonstrate the efficacy of our method with numerical experiments.

Key words: Multilevel quasi Monte Carlo, white noise, non-nested meshes, Matérn Gaussian fields, finite elements, partial differential equations with random coefficients, low-discrepancy sequences

1 Introduction

In this paper we extend the work of [13] to the quasi and multilevel quasi Monte Carlo case (QMC and MLQMC respectively). We consider the solution of random elliptic partial differential equations (PDEs) in which Matérn fields, sampled via the stochastic PDE (SPDE) approach [46], appear as coefficients. For instance, a typical problem is: find $\mathbb{E}[P]$, where $P(\omega) = \mathcal{P}(p)$ and \mathcal{P} is a Fréchet differentiable functional of the function p that satisfies,

$$-\nabla \cdot (F(u(\mathbf{x}, \omega)) \nabla p(\mathbf{x}, \omega)) = f(\mathbf{x}), \quad \mathbf{x} \in G \subset \mathbb{R}^d, \quad \omega \in \Omega, \quad (1)$$

***Funding:** This research is supported by EPSRC grants EP/R029423/1, and by the EPSRC Centre For Doctoral Training in Industrially Focused Mathematical Modelling (EP/L015803/1).

[†]Mathematical Institute, University of Oxford, Oxford, UK. (matteo.croci@maths.ox.ac.uk), (patrick.farrell@maths.ox.ac.uk), (mike.giles@maths.ox.ac.uk).

with suitable boundary conditions. Here we take the function f and the domain G to be suitably smooth and $F \in C^0(\mathbb{R})$ to be a positive locally Lipschitz function. In this work, we assume that the coefficient $u(\mathbf{x}, \omega)$ is a zero-mean Matérn field approximately sampled by solving the (domain-truncated) Whittle SPDE [46, 55]:

$$(\mathcal{I} - \kappa^{-2}\Delta)^k u(\mathbf{x}, \omega) = \eta \dot{W}, \quad \mathbf{x} \in D \subset \mathbb{R}^d, \quad \omega \in \Omega, \quad \nu = 2k - d/2 > 0, \quad (2)$$

where \dot{W} is spatial Gaussian white noise in \mathbb{R}^d , and $k > d/4$. Here $d \leq 3$ and the equality has to hold almost surely and be interpreted in the sense of distributions. The constant $\eta > 0$ is a scaling factor that depends on σ , λ and ν , cf. [13]. In what follows we assume that $G \subset\subset D \subset\subset \mathbb{R}^d$, where by $G \subset\subset D$ we indicate that the closure of G is a compact subset of D , and we prescribe homogeneous Dirichlet boundary conditions on ∂D . If the distance between ∂D and ∂G is large enough, then the error introduced by truncating \mathbb{R}^d to D is negligible [39, 56].

A wide range of Gaussian field sampling methods are available in the literature. The simplest of them all involves a Cholesky factorization of the covariance matrix of the Gaussian vector $\mathbf{u}(\omega) = [u(\mathbf{x}_1, \omega), \dots, u(\mathbf{x}_m, \omega)]^T$ containing the values of the field $u(\mathbf{x}, \omega)$ at $m \in \mathbb{N}^+$ discrete locations $\mathbf{x}_i \in D$. Indicating with $C \in \mathbb{R}^{m \times m}$ the typically dense, positive-definite covariance matrix of \mathbf{u} , a sample of \mathbf{u} can be obtained by first computing a Cholesky factorization $C = HH^T$ and then setting $\mathbf{u} = H\mathbf{z}$ for a given sample of a standard Gaussian vector $\mathbf{z} \sim \mathcal{N}(0, I)$, $\mathbf{z} \in \mathbb{R}^m$. The total cost of this sampling strategy is a $O(m^3)$ cost for the factorization and a $O(m^2)$ cost per sample.

More efficient methods are available. The most common are: the Karhunen-Loève expansion of the random field (cf. section 11.1 in [58]); the hierarchical matrix approximation of the covariance matrix [17, 22, 31, 38]; the circulant embedding method [1, 16, 28, 60]; the SPDE approach [13, 46, 55]. Each of these methods has its advantages and disadvantages and is more or less efficient according to the covariance structure of the field. We do not describe these methods further here, but we refer to section 2.4 in [11] for a more detailed overview and comparison. In this paper, we only consider the SPDE approach, which consists of sampling a Matérn field by solving equation (2) for a given realization of white noise. Equation (2) can be solved after discretization in $O(m)$ cost complexity with an optimal solver. This yields an overall $O(m)$ sampling complexity provided that the white noise term can also be sampled in linear cost. In [13], the authors have showed how white noise realizations can be sampled in $O(m)$ complexity within a finite element (FEM) and non-nested MLMC framework.

The new (ML)QMC method we present in this paper is based on the efficient sampling of the white noise term in (2) with a hybrid quasi/pseudo-random sequence. It is extremely important for QMC applications for the QMC integrand to have low effective dimensionality and to order the QMC integrand variables in order of decaying importance [8]. For this reason, a common approach in the existing literature about MLQMC methods for elliptic PDEs is the expansion of the random field coefficients as an infinite series of basis functions of $L^2(D)$ that naturally exposes the leading order dimensions in the integrands [15, 29, 41, 42]. If the random field is smooth, the coefficients in the (e.g. Karhunen-Loève) expansion quickly decay and a truncated expansion provides both the variable ordering and the low-effective dimensionality required by QMC methods.

When using the SPDE approach and equation (2), the only source of randomness is white noise and we therefore must expand \dot{W} to achieve the required variable ordering. In this case, the Karhunen-Loève expansion does not provide a feasible route since white noise is not smooth and the eigenvalues in the expansion do not decay. A good alternative in this case is offered by a wavelet expansion of \dot{W} .

Wavelets in general form a multi-resolution orthogonal basis of $L^2(D)$ and are commonly employed within QMC algorithms as their hierarchical structure exposes the leading order dimensions in the integrands while allowing fast $O(m)$ or $O(m \log m)$ complexity operations (depending on the wavelet basis [14]). A classical example on the efficacy of wavelet expansions of white noise (in time) within a QMC method is offered by the Lévy-Ciesielski (or Brownian bridge) construction of Brownian motion. Ubiquitous in mathematical finance, it is commonly used to solve stochastic differential equations with QMC [24, 27]. Inspired by this technique, we choose to expand white noise into a Haar wavelet expansion¹, although the generalization of our approach to higher degree wavelets should be straight-forward.

In a MLQMC framework, wavelets are used by Kuo et al. to sample random fields efficiently, yielding a cost per sample of $O(m \log m)$ using nested grids [41]. In [34], Hermann and Schwab use a truncated wavelet expansion of white noise to sample Gaussian fields with the SPDE approach within a nested MLQMC hierarchy. Their work is possibly the closest to ours as they also work with the SPDE approach to Matérn field sampling and use a wavelet expansion of white noise [34].

Generally speaking, all the randomized MLQMC methods for elliptic PDEs presented in the above papers are strongly theory-oriented. They use randomly shifted lattice rules and derive MLQMC complexity bounds using a pure QMC approach, truncated expansions and nested hierarchies on simple geometries. Our work is different in spirit and strategy. Firstly, our focus is practice-oriented and we do not derive any MLQMC complexity estimates, but we design our method to work in the general case in which the multilevel hierarchy is non-nested and the domain geometries are non-trivial. Secondly, we handle the expansion differently: we do not just truncate it, but we work with the whole infinite expansion of white noise by adding a correction term to the truncation. The truncation term is finite-dimensional and we sample it with a randomized low-discrepancy sequence; the correction term is infinite-dimensional and a QMC approach is not feasible. However, the covariance of the correction is known and we can sample it using pseudo-random numbers with an extension of the technique presented in [13]. We can still sample white noise (and consequently the Matérn field) in linear cost complexity (or log-linear, according to the Haar wavelet type) as in [13].

We therefore adopt a hybrid MC/QMC approach. The advantage of doing so is that we can sample white noise exactly, independently from the truncation level and the wavelet degree considered (e.g. while we use Haar wavelets, Hermann and Schwab in [34] consider higher degree wavelets), without introducing any additional bias into the MLQMC estimate. In contrast, in the aforementioned MLQMC algorithms the expansion must be truncated after enough terms to make the truncation error negligible. Naturally, this advantage comes at a price: since we are using pseudo-random numbers as well, the asymp-

¹Note that the hat functions used in the Lévy-Ciesielski construction are piecewise linear wavelets, their derivatives are Haar wavelets and white noise in time is the derivative of Brownian motion.

otic convergence rate of our method with respect to the number of samples N is still the standard MC rate of $O(N^{-1/2})$. Nevertheless, we show that large computational gains can be recovered in practice in a pre-asymptotic QMC-like regime in which the convergence rate is $O(N^{-\chi})$, $\chi \geq 1/2$, and we derive a partial convergence result (cf. supplementary material) that explains this behaviour in the QMC case.

Wavelets are used in both [41] and [34], but no comment is made about how to work with the wavelet basis in practice if this is not nested within the FEM approximation subspace. This happens whenever the mesh on which we solve the Whittle SPDE (2) is non-uniform. When working with complex geometries and graded meshes it is desirable for the sampled Matérn field to have the same accuracy as the solution of the PDE of interest (e.g. (1)) and the Matérn field should not therefore be sampled on a uniform structured mesh. For this purpose, we adopt the embedded mesh technique by Osborn et al. [50] so that in the MLQMC hierarchy each mesh of G is nested within the corresponding mesh of D and we deal with the non-nestedness of the FEM and wavelet spaces via a supermesh construction.

In the independent white noise realization case we construct a two-way supermesh between the graded FEM mesh of interest and a uniform “wavelet” mesh and we sample white noise in a consistent way between the FEM and the wavelet subspaces. In the MLQMC coupled realization case, we construct a three-way supermesh between the two non-nested FEM meshes and the “wavelet” mesh. The supermesh constructions can be simplified when the meshes involved are nested and if all meshes are nested no supermesh is required. In any case, the number of supermesh cells is still linear in the number of cells of the parent meshes under mild assumptions [12]. We remark that the same supermeshing strategy can be employed to sample the truncated white noise expansion used in [34] in the general non-uniform case as our technique easily generalises to higher degree wavelets.

This paper is structured as follows: in section 2 we summarize the mathematical background needed to understand the rest of the paper. In section 3 we introduce the Haar wavelet expansion of white noise and its splitting into a truncated term and a correction term. In section 4 we introduce our sampling technique for independent white noise realizations. We extend the white noise sampling method to MLQMC in section 5, where we show how coupled white noise realizations can be sampled efficiently. The algorithms are supported by numerical results, which we present and discuss in section 6. We conclude the paper with a brief summary of the methods and results presented in section 7.

2 Notation and background

2.1 Notation

In this paper we denote with $L^2(D)$ the space of square-integrable functions over D and with (\cdot, \cdot) the standard $L^2(D)$ inner product. We furthermore indicate with $W^{k,q}(D)$ the standard Sobolev space of integrability order q and differentiability k , with $H^k(D) \equiv W^{k,2}(D)$ and with $H_0^1(D)$ the space of $H^1(D)$ functions that vanish on ∂D in the sense of traces.

Given a sample space Ω , we indicate with $L^2(\Omega, \mathbb{R})$ the space of real-valued *random variables* with finite second moment.

For a given Banach space U over D , we indicate with $L^2(\Omega, U)$ the space of *random fields* $u(\mathbf{x}, \omega)$, $\mathbf{x} \in D$, $\omega \in \Omega$ such that $u(\mathbf{x}, \cdot) \in L^2(\Omega, \mathbb{R})$ for almost every $\mathbf{x} \in D$ and $u(\cdot, \omega) \in U$ almost surely (a.s.). If the $u(\mathbf{x}, \cdot)$ are jointly Gaussian for almost every $\mathbf{x} \in D$, then the random field is a *Gaussian field* and it is uniquely determined by its mean $\mu(\mathbf{x})$ and covariance $C(\mathbf{x}, \mathbf{y})$ functions. Throughout this paper we will consider only zero-mean fields for simplicity.

A Gaussian field is also a *Matérn field* if its covariance is of the Matérn class, i.e.

$$C(\mathbf{x}, \mathbf{y}) = \frac{\sigma^2}{2^{\nu-1}\Gamma(\nu)} (\kappa r)^\nu \mathcal{K}_\nu(\kappa r), \quad r = \|\mathbf{x} - \mathbf{y}\|_2, \quad \kappa = \frac{\sqrt{8\nu}}{\lambda}, \quad \mathbf{x}, \mathbf{y} \in D, \quad (3)$$

where σ^2 , ν , $\lambda > 0$ are the variance, smoothness parameter and correlation length of the field respectively, $\Gamma(x)$ is the Euler Gamma function and \mathcal{K}_ν is the modified Bessel function of the second kind.

In this paper we will adopt the following definition of *generalized random field*, first introduced by Itô [40] and extended by Inaba and Tapley [36]. For a given Banach space U , we denote with $\mathcal{L}(U, L^2(\Omega, \mathbb{R}))$ the space of generalized random fields that are continuous linear mappings from U to $L^2(\Omega, \mathbb{R})$. For a given $\xi \in \mathcal{L}(U, L^2(\Omega, \mathbb{R}))$ we indicate the action (or pairing) of ξ onto a function $\phi \in U$ with the notation $\xi(\phi) = \langle \xi, \phi \rangle$.

Possibly the most commonly used generalized random field is Gaussian *white noise*. White noise is defined as follows.

Definition 2.1 (White noise, see example 1.2 and lemma 1.10 in [35]). Let $D \subseteq \mathbb{R}^d$ be an open domain. The white noise $\dot{W} \in \mathcal{L}(L^2(D), L^2(\Omega, \mathbb{R}))$ is a generalized stochastic field such that for any collection of $L^2(D)$ functions $\{\phi_i\}$, if we let $b_i = \langle \dot{W}, \phi_i \rangle$, then $\{b_i\}$ are joint Gaussian random variables with zero mean and covariance given by $\mathbb{E}[b_i b_j] = (\phi_i, \phi_j)$.

2.2 Randomized quasi Monte Carlo

Quasi Monte Carlo Quasi Monte Carlo (QMC) methods retain most of the advantages of standard Monte Carlo (MC) while improving the convergence order with respect to the number of samples. At the heart of QMC for estimating expectations is the reinterpretation/approximation of the expected value as an integral with respect to the uniform distribution over the unit hypercube:

$$\mathbb{E}[P] = \int_{\Omega} P(\omega) d\mathbb{P}(\omega) \approx \int_{[0,1]^s} Y(\mathbf{x}) d\mathbf{x}, \quad (4)$$

for some suitable function Y . Here \mathbb{P} is the probability measure of a suitable probability space $(\Omega, \mathcal{A}, \mathbb{P})$, with \mathcal{A} as its σ -algebra.

QMC methods are, in fact, nothing but quadrature rules over the unit hypercube with N points and equal weights, approximating the integral on the right-hand side as

$$I = \int_{[0,1]^s} Y(\mathbf{x}) d\mathbf{x} \approx \frac{1}{N} \sum_{n=1}^N Y(\mathbf{x}_n) = I_N, \quad (5)$$

where the $\mathbf{x}_n \in \mathbb{R}^s$ are, unlike in the standard MC case, not chosen at random, but chosen carefully and in a deterministic way so as to minimise a quantity called the *discrepancy* of the point set. Informally, discrepancy is a measure of how well the point sequence covers the unit hypercube (cf. figure 1) and its importance lies in the fact that the QMC quadrature error decays proportionally to the discrepancy as N increases [42, 43, 49].

While random sequences are proven to have discrepancy of $O((\log \log N/N)^{1/2})$ with probability one [49], there exist deterministic sequences that achieve discrepancies of $O((\log N)^s/N)$ [49]. These sequences are called *low-discrepancy* point sequences and, if used for QMC integration, yield a faster-than-MC asymptotic rate of $O(N^{-1+\epsilon})$, for any $\epsilon > 0$, provided that the integrand Y is smooth enough.

Unlike standard MC, QMC methods are not completely dimension-independent: for high-dimensional problems the $(\log N)^s$ term in the discrepancy might dominate for small sample sizes. If this happens, low-discrepancy sequences cease to cover the whole hypercube well and their discrepancy temporarily falls back to a $O(N^{-1/2})$ rate² as in the random case up until N becomes impractically huge [8]. However, this is not always the case. Caffish et al. in [8] investigate this behaviour and introduce the notion of *low effective dimensionality*: if the QMC integrand can be well approximated by a function that only depends on the first $\bar{s} \ll s$ QMC variables, the $(\log N)^s$ in the discrepancy bound can be replaced with $(\log N)^{\bar{s}}$, for which the transition to a $O(N^{-1})$ -like regime will already happen for small sample sizes [8]. More recent theoretical results on QMC convergence [28, 34, 41, 42] adopt a slightly different interpretation of low effective dimensionality and work with the underlying assumption that there is “*some varying degree of importance between the variables*” [43]. This yields dimension-independent error bounds.

Overall, for practical applications of high-dimensional QMC integration it is extremely important to order the integration variables in order of decaying importance and/or reduce the dimensionality of the integrand so that higher-than-MC convergence rates can be achieved. This will be a key aspect in the methods we present in this paper.

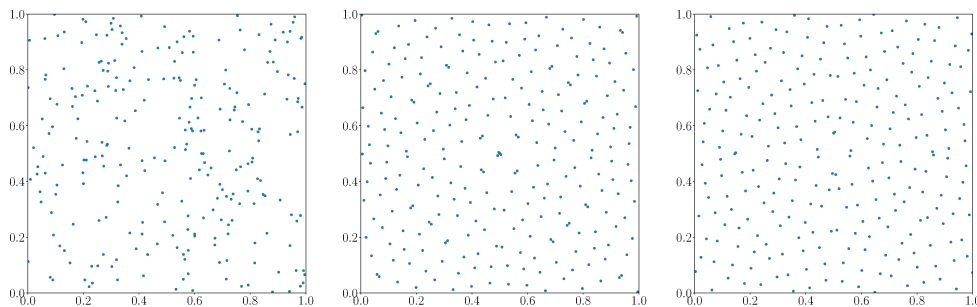


Figure 1: *Pseudo-random, not randomized and randomized low-discrepancy sequences in comparison. On the left, a sample of 256 uniform random points. In the middle, the first 256 points in a 2-dimensional Sobol’ sequence. On the right, the same points after random digital shifting. The low-discrepancy sequence covers the unit square better than the pseudo-random sequence, even after randomization.*

²Caffish et al. also report that QMC integration is almost never worse than standard MC [8].

Randomized quasi Monte Carlo Although theoretically useful, a bound depending on a discrepancy measure cannot be used in practice as the discrepancy value is extremely difficult to estimate. Furthermore, low-discrepancy sequences are deterministic and we cannot rely on the central limit theorem as for standard MC.

Randomized QMC methods combine MC and QMC ideas and fix these issues by randomising the low-discrepancy sequence used, i.e. given a fixed deterministic low-discrepancy sequence $\{\mathbf{x}_n\}_{n=1}^N$, randomized QMC produces a set of M independent randomized sequences $\{\hat{\mathbf{x}}_{n,m}(\omega)\}_{n=1,m=1}^{n=N,m=M}$ in such a way that the discrepancy properties of the parent sequence are preserved (see figure 1). See chapter 6 of [45] for an overview and [54] for a comparison of various randomization techniques. The randomized sequences are then combined into the randomized QMC estimator,

$$\hat{I}_{M,N}(\omega) = \frac{1}{M} \sum_{m=1}^M I_N^m(\omega) = \frac{1}{M} \sum_{m=1}^M \left(\frac{1}{N} \sum_{n=1}^N Y(\hat{\mathbf{x}}_{n,m}(\omega)) \right). \quad (6)$$

Since $I_N^m(\omega)$ is now random, provided that M is large enough a confidence interval can be estimated and we retain a practical error measure as in the standard MC case. In this work we use $M = 32$ unless otherwise stated. Assuming fixed M , a given mean square error (MSE) tolerance ε^2 , a $O(\varepsilon^{-q})$ cost per sample and a QMC convergence order of $O(N^{-1+\epsilon})$ for any $\epsilon > 0$, the total cost of randomized QMC is $O(\varepsilon^{-q-1/(1-\epsilon)})$, which for small ϵ is almost ε^{-1} times better than standard MC.

2.3 Multilevel Monte Carlo methods

The multilevel Monte Carlo method was first introduced by Heinrich in [33] for parametric integration and popularised by Giles for stochastic differential equations in [26]. Multilevel quasi Monte Carlo, originally presented in [24], combines QMC and MLMC together with the objective of combining their advantages. Assume that it is possible to compute realizations of $P(\omega)$ at different accuracy levels $P_\ell(\omega)$ for $\ell = 1, \dots, L$ of increasing accuracy and computational cost, and that the approximation of P on the finest level, P_L is accurate enough. Multilevel methods estimate $\mathbb{E}[P_L]$ through the telescopic sum,

$$\mathbb{E}[P] \approx \mathbb{E}[P_L] = \sum_{\ell=1}^L \mathbb{E}[P_\ell - P_{\ell-1}], \quad (7)$$

where $P_0 \equiv 0$. For example, if samples of P are obtained by solving (1) with the FEM, the levels of accuracy can be defined by using a hierarchy of meshes (h -refinement) or by increasing the polynomial degree of the finite element bases used (p -refinement).

The MLMC and MLQMC estimators are then obtained from (7) by approximating each term in the sum with standard MC or randomized QMC respectively. For MLMC we have,

$$\mathbb{E}[P_\ell - P_{\ell-1}] \approx \frac{1}{N_\ell} \sum_{n=1}^{N_\ell} (P_\ell - P_{\ell-1})(\omega_\ell^n), \quad (8)$$

in which each $P_\ell - P_{\ell-1}$ sample is coupled in the sense that the samples of P_ℓ and $P_{\ell-1}$ share the same event ω_ℓ^n . Ensuring this coupling is respected in practice is essential for

any MLMC algorithm since this coupling is the reason behind the increased efficiency of MLMC with respect to standard MC [26].

Enforcing the same type of coupling is also essential for MLQMC. In the MLQMC case each term in (7) is approximated with randomized QMC as follows,

$$\mathbb{E}[P_\ell - P_{\ell-1}] = \int_{[0,1]^{s_\ell}} Y_\ell(\mathbf{x}) d\mathbf{x} \approx \frac{1}{M} \sum_{m=1}^M \left(\frac{1}{N_\ell} \sum_{n=1}^{N_\ell} Y_\ell(\hat{\mathbf{x}}_{n,m}^\ell(\omega)) \right) = \frac{1}{M} \sum_{m=1}^M I_{N_\ell}^{m,\ell}(\omega), \quad (9)$$

where the meaning of each variable is the same as in the QMC case. Note that the multilevel coupling is implicit in the fact that Y_ℓ now represents the difference $P_\ell - P_{\ell-1}$. We now have a hierarchy of integrands $\{Y_\ell\}_{\ell=1}^L$ and of randomized low-discrepancy sequences $\{\hat{\mathbf{x}}_{n,m}^\ell\}_{n=1, m=1, \ell=1}^{n=N_\ell, m=M, \ell=L}$ of dimensions $\{s_\ell\}_{\ell=1}^L$. Note that, in the same way as for QMC, MLQMC still requires for good performance either the integration variables on each level to be organized in order of decaying importance or the integrands Y_ℓ to have low effective dimensionality.

The theory for MLMC is by now established [9, 26, 59], yielding formulas for the optimal number of samples N_ℓ on each level and for the total MLMC algorithm complexity ($O(\varepsilon^{-2})$ in the best case scenario, see supplementary material A). On the other hand, proving any convergence result for MLQMC is particularly hard, to the extent that convergence proofs are only available for a few specific problems and specific low-discrepancy sequences [34, 42]. For this reason, setting up an optimal MLQMC hierarchy with the optimal values of the N_ℓ is a challenging task. However, in the best possible case where we get a $O(N^{-\chi})$, $1/2 \leq \chi \leq 1$, QMC rate for each term in the telescoping sum, the benefits of MLMC and QMC can accumulate yielding a total MLQMC computational cost of $O(\varepsilon^{-1/\chi})$ for a given MSE tolerance of ε^2 [34]. In this case MLQMC significantly outperforms all other Monte Carlo methods.

In this paper we employ the original MLQMC algorithm from [24] as it does not require the convergence rate with respect to N to be known *a priori*. We refer to the supplementary material A for a description of the algorithm.

2.4 Supermeshes

We now introduce the concepts of non-nested tessellations/meshes and of a supermesh.

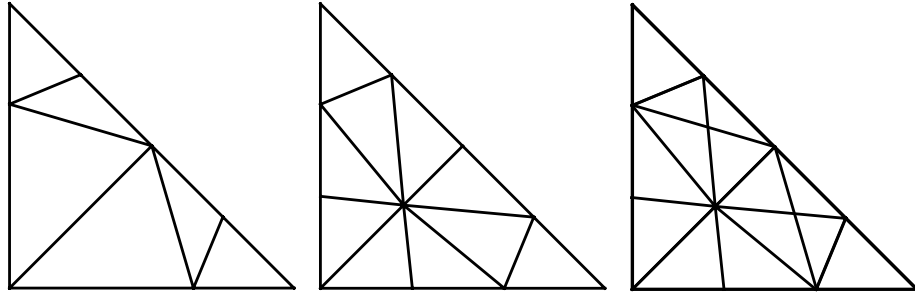


Figure 2: An example of a supermesh construction. The first two meshes on the left are the parent meshes and the mesh on the right is one of their supermeshes.

Let T_a and T_b be two tessellations of D . We say that T_a is *nested* within T_b if $\text{vertices}(T_a) \subseteq \text{vertices}(T_b)$ and if for each element $e \in T_a$ there exists a set of elements $E \subseteq T_b$ such that $e = \bigcup_{\hat{e}_i \in E} \hat{e}_i$. We say that T_a and T_b are *non-nested* if T_a is not nested within T_b and vice-versa.

A crucial ingredient we need to enforce the multilevel (quasi) Monte Carlo coupling across a non-nested mesh hierarchy is a supermesh construction. Supermeshes are commonly used e.g. within adaptive discretizations or geometric multigrid algorithms, to transfer discrete fields between non-nested meshes [21]. A supermesh is defined as follows.

Definition 2.2 (Supermesh, [20, 21]). Let $D \subset \mathbb{R}^d$ be an open domain and let $\mathcal{T}_a, \mathcal{T}_b$ be two tessellations of D . A supermesh S_h of \mathcal{T}_a and \mathcal{T}_b is a common refinement of \mathcal{T}_a and \mathcal{T}_b . More specifically, S_h is a triangulation of D such that:

1. $\text{vertices}(\mathcal{T}_a) \cup \text{vertices}(\mathcal{T}_b) \subseteq \text{vertices}(S_h)$,
2. $\text{measure}(e_S \cap e) \in \{0, \text{measure}(e_S)\}$ for all cells $e_S \in S_h$, $e \in (\mathcal{T}_a \cup \mathcal{T}_b)$.

The first condition means that every parent mesh vertex must also be a vertex of the supermesh, while the second states that every supermesh cell is completely contained within exactly one cell of either parent mesh [21]. The supermesh construction is not unique [21]. We show an example of supermesh construction in figure 2. Efficient algorithms for computing the supermesh are available [48].

It was shown in [12] that if the parent tessellations T_a and T_b are quasi-uniform (cf. definition 4.4.13 in [7]), then the number of cells of a supermesh constructed via a local supermeshing algorithm (cf. [19]) is linear in the number of cells of T_a and T_b .

3 Haar wavelet expansion of spatial white noise

For good QMC convergence we need to order the dimensions of the QMC integrand in order of decaying importance so that the largest error components are on the leading dimensions [15, 27]. In what follows we expand white noise into a Haar wavelet series so that the hierarchical structure of Haar wavelets can naturally provide the variable ordering needed for QMC integration.

We start by introducing the Haar wavelet basis. Let $\mathbb{1}_A(x)$ be the indicator function of a set A and let $\Psi(x)$ for $x \in \mathbb{R}$ be the Haar mother wavelet,

$$\Psi(x) = \mathbb{1}_{[0,1/2)}(x) - \mathbb{1}_{[1/2,1)}(x) = \begin{cases} 1, & 0 \leq x < 1/2, \\ -1, & 1/2 \leq x < 1, \\ 0, & \text{otherwise.} \end{cases} \quad (10)$$

Let $\bar{\mathbb{N}} = \{-1\} \cup \mathbb{N}$ and let $x^+ = \max(x, 0)$. The Haar wavelets $H_{l,n}$ for $l \in \bar{\mathbb{N}}$, $n = 0, \dots, 2^{l^+} - 1$ can be expressed in terms of the mother wavelet through shifting and rescaling as follows.

$$\begin{cases} H_{-1,0}(x) = \mathbb{1}_{[0,1)}(x), & l = -1, n = 0 \\ H_{l,n}(x) = 2^{l/2} \Psi(2^l x - n), & l \in \mathbb{N}, n = 0, \dots, 2^l - 1. \end{cases} \quad (11)$$

The Haar wavelets have support size $|\text{supp}(H_{\mathbf{l},\mathbf{n}})| = 2^{-\mathbf{l}^+}$ and form an orthonormal basis of $L^2(0,1)$. The Haar system can be generalized to higher dimensions by taking the tensor product of the 1D Haar basis with itself: let $\mathbf{l} \in \bar{\mathbb{N}}^d$ and $\mathbf{n} \in \mathbb{N}$ we can define the family of d -dimensional Haar wavelets $H_{\mathbf{l},\mathbf{n}}(\mathbf{x})$ for $\mathbf{x} \in \mathbb{R}^d$ as

$$H_{\mathbf{l},\mathbf{n}}(\mathbf{x}) = \bigotimes_{i=1}^d H_{l_i, n_i}(x_i), \quad \text{with } n_i \in \{0, \dots, 2^{l_i^+} - 1\} \forall i. \quad (12)$$

The d -dimensional Haar wavelets have support size $|\text{supp}(H_{\mathbf{l},\mathbf{n}})| = \prod_{i=1}^d 2^{-l_i^+} = 2^{-\|\mathbf{l}^+\|_1}$ and they form an orthonormal basis of $L^2((0,1)^d)$. It is also possible to construct an orthonormal basis of L^2 for a general boxed (hyper-rectangular) domain by scaling and shifting the components of \mathbf{x} accordingly.

Remark 3.1 (On the non-standard Haar wavelet basis). The d -dimensional wavelets just introduced are sometimes called the *standard* Haar basis, which leads to log-linear complexity operations (rather than just linear) for $d > 1$. Even though this is the basis we use in our numerical experiments, the algorithms we will introduce also work for the *non-standard* Haar basis, which supports linear complexity operations in all dimensions [4, 14].

Let $z_{\mathbf{l},\mathbf{n}}(\omega)$ be i.i.d. standard normal random variables. Furthermore, let $|\mathbf{l}| = \max_i(l_i)$. We can express white noise over $[0,1]^d$ as a Haar wavelet expansion,

$$\dot{W} = \sum_{|\mathbf{l}|=-1}^{|\mathbf{l}|=\infty} \sum_{\mathbf{n}=0}^{2^{\mathbf{l}^+}-1} z_{\mathbf{l},\mathbf{n}}(\omega) H_{\mathbf{l},\mathbf{n}}(\mathbf{x}). \quad (13)$$

The second summation is to be interpreted as the sum over all \mathbf{n} with components n_i such that $0 \leq n_i \leq 2^{l_i^+} - 1$ for all i . Let $\mathcal{L} \in \bar{\mathbb{N}}$. We now divide the series in two terms,

$$\dot{W} = \dot{W}_{\mathcal{L}} + \dot{W}_R = \sum_{|\mathbf{l}|=-1}^{|\mathbf{l}|=\mathcal{L}} \sum_{\mathbf{n}=0}^{2^{\mathbf{l}^+}-1} z_{\mathbf{l},\mathbf{n}}(\omega) H_{\mathbf{l},\mathbf{n}}(\mathbf{x}) + \sum_{|\mathbf{l}|=\mathcal{L}+1}^{|\mathbf{l}|=\infty} \sum_{\mathbf{n}=0}^{2^{\mathbf{l}^+}-1} z_{\mathbf{l},\mathbf{n}}(\omega) H_{\mathbf{l},\mathbf{n}}(\mathbf{x}). \quad (14)$$

The idea is then to sample the Gaussian variables in the expression for $\dot{W}_{\mathcal{L}}$ by using a hybrid QMC/MC combination of quasi-random (e.g. Sobol) and pseudo-random numbers, and to sample \dot{W}_R with pseudo-random numbers only by extending the work in [13].

The reasoning behind this splitting is that it is important to keep the dimensionality of the low-discrepancy sequence relatively low: first, as we will see in the next section, the sampling of \dot{W} expressed this way requires a supermesh construction and smaller dimensions imply faster \dot{W} samples; second, some low-discrepancy sequences cannot readily be sampled in high dimensions³ and third, the approximation properties of some quasi-random sequences deteriorate as the dimensionality grows [15, 27].

³For example, the state-of-the-art Sobol' sequence generator, Broda, can generate the largest dimensional Sobol' sequences with 65536 dimensions [57]. This might still be too low for an infinite-dimensional PDE setting.

4 Sampling independent realizations for QMC

To sample $u(\mathbf{x}, \omega)$, we must solve equation (2). In what follows, we set $\eta = 1$ and we will only consider the $k = 1$ case for simplicity. We refer to [6], [5] for the general $k > d/4$ case. After these simplifications, we obtain

$$\begin{aligned} u - \kappa^{-2} \Delta u &= \dot{W}, \quad \mathbf{x} \in D, \\ u &= 0, \quad \mathbf{x} \in \partial D. \end{aligned} \tag{15}$$

From now on we introduce the simplifying assumption that $D = [0, 1]^d$. Relaxing this assumption to general boxed domains is straightforward, but considering more general cases is non-trivial. As we are using the SPDE approach, we are free to choose any domain shape for D [46] so this is not really a restriction. It is useful for what comes next to introduce the concept of a Haar mesh (see figure 3a):

Definition 4.1 (Haar mesh). Let $D = [0, 1]^d$ and let $\mathcal{L} \in \bar{\mathbb{N}}$. The Haar mesh $D_{\mathcal{L}}$ is the uniform quadrilateral mesh of D whose cells are all regular polyhedra of volume $|\square_H| = 2^{-d(\mathcal{L}+1)}$. Note that for a given \mathcal{L} there are exactly as many cells in $D_{\mathcal{L}}$ as terms in the wavelet expansion (14) for $\dot{W}_{\mathcal{L}}$, namely $N_{\mathcal{L}} = 2^{d(\mathcal{L}+1)}$.

We solve (15) with the FEM. Let D_h be a mesh of D , not necessarily nested within the Haar mesh $D_{\mathcal{L}}$. Let $V \subseteq H_0^1(D)$ and let $V_h = \text{span}(\phi_1, \dots, \phi_m) \subseteq V$ be the FEM subspace used to solve equation (15) on D_h . In what follows we will refer to D_h as the *FEM mesh* and we assume for simplicity that there are always m_e degrees of freedom of V_h on each cell of D_h .

A discrete weak form of (15) then reads: find $u_h \in V_h$ such that

$$(u_h, v_h) + \kappa^{-2} (\nabla u_h, \nabla v_h) = \langle \dot{W}, v_h \rangle \quad \text{for all } v_h \in V_h. \tag{16}$$

The solution $u_h = \sum_{i=1}^m u_i \phi_i$, expressed in terms of the basis functions of V_h , is given by the following linear system for the u_i ,

$$A \mathbf{u} = \mathbf{b}, \quad \text{where} \quad A_{ij} = (\phi_i, \phi_j) + \kappa^{-2} (\nabla \phi_i, \nabla \phi_j), \quad b_i = \langle \dot{W}, \phi_i \rangle. \tag{17}$$

Now, since $\dot{W} = \dot{W}_{\mathcal{L}_\ell} + \dot{W}_R$, the b_i can also be expressed as

$$b_i = (\mathbf{b}_{\mathcal{L}})_i + (\mathbf{b}_R)_i, \quad \text{with} \quad (\mathbf{b}_{\mathcal{L}})_i = \langle \dot{W}_{\mathcal{L}}, \phi_i \rangle, \quad (\mathbf{b}_R)_i = \langle \dot{W}_R, \phi_i \rangle, \tag{18}$$

Note that we use the $L^2(D)$ inner product notation for $\dot{W}_{\mathcal{L}}$ since $\dot{W}_{\mathcal{L}}$ is a.s. in $L^2(D)$ for finite \mathcal{L} .

The task of computing a realization of white noise is therefore equivalent to computing a sample of $\dot{W}_{\mathcal{L}}$ and \dot{W}_R , and consequently of the two vectors $\mathbf{b}_{\mathcal{L}}$ and \mathbf{b}_R . As we will see, the sampling strategies for the two terms are considerably different. Nevertheless, we will explain how both terms can be sampled efficiently in linear or log-linear complexity.

Remark 4.1. From now on we assume without loss of generality that the support of each $\phi_i \in V_h$ is entirely contained in a single Haar mesh cell. The reason why the generality of what follows is not affected is that each basis function $\phi_i \in V_h$ can always be split into the sum of the restrictions of ϕ_i to each cell of $D_{\mathcal{L}}$. Note that splitting the basis functions when D_h is non-nested within the Haar mesh requires a supermesh construction. We will indicate with S_h a given supermesh between D_h and $D_{\mathcal{L}}$.

4.1 Sampling of $\dot{W}_{\mathcal{L}}$

We first consider the efficient sampling of $\dot{W}_{\mathcal{L}}$. In order to achieve good convergence with respect to the number of QMC samples we align the terms in the quasi-random sequence according to the $\|\cdot\|_1$ norm of the vector \mathbf{l} in the expansion (14) for $\dot{W}_{\mathcal{L}}$: the first term corresponds to $z_{-1,0}$, the second batch of terms corresponds to the $z_{\mathbf{l},n}$ with $\|\mathbf{l}\|_1 = 0$, the third batch to those with $\|\mathbf{l}\|_1 = 1$ and so on.

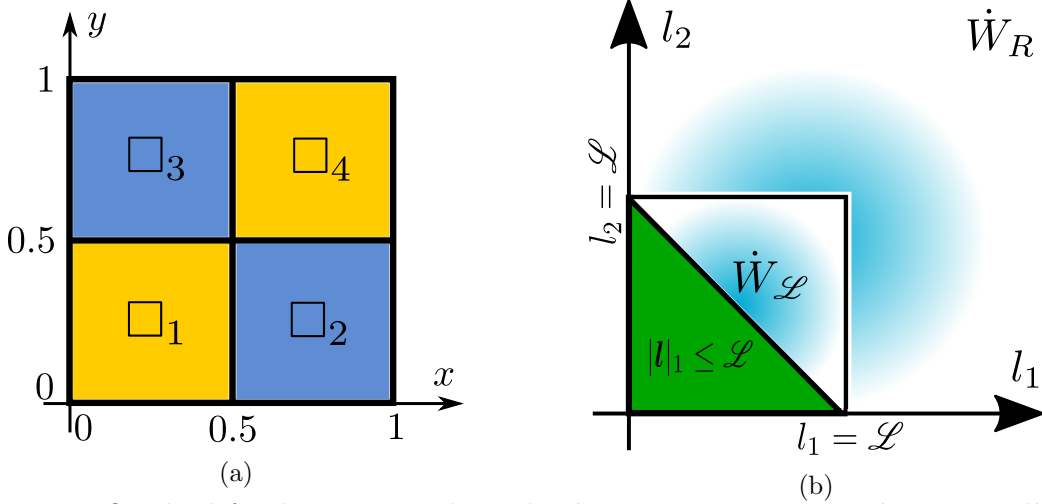


Figure 3: On the left, the Haar mesh in the $d = 2$, $\mathcal{L} = 0$ case. The Haar cells are coloured according to the values of the $H_{\mathbf{0},\mathbf{0}} = \Psi(x)\Psi(y)$ wavelet: yellow for $+1$, blue for -1 . On the right, a schematic of the sampling strategy for the Haar coefficients of \dot{W} in 2D. The coefficients in the square are the coefficients for $\dot{W}_{\mathcal{L}}$, while those in the unbounded “L-shaped” domain belong to \dot{W}_R . The green region corresponds to the coefficients with $\|\mathbf{l}\|_1 \leq \mathcal{L}$ which are sampled with a low-discrepancy sequence and ordered according to $\|\mathbf{l}\|_1$. The others, corresponding to the light blue regions, are sampled with independent pseudo-random numbers.

We adopt a hybrid sampling technique for $\dot{W}_{\mathcal{L}}$: of all the wavelet coefficients $z_{\mathcal{L}} \in \mathbb{R}^{N_{\mathcal{L}}}$ corresponding to the Haar levels $|\mathbf{l}| \leq \mathcal{L}$, we only sample those with $\|\mathbf{l}\|_1 \leq \mathcal{L}$ (note the change from max norm to 1 norm) using a low-discrepancy sequence (in our case Sobol with digital shifting [27]) and we sample the rest using independent pseudo-random numbers, i.e. we sample $z_{\mathcal{L}} = [z_{\text{QMC}}^T, z_{\text{MC}}^T]^T$, where z_{QMC} is obtained by applying the normal inverse CDF to a randomized low-discrepancy sequence point and z_{MC} is sampled with a pseudo-random number generator. Again this is in the interest of keeping the dimensionality of the low-discrepancy sequence low. To get an idea of the numbers, there are $2^{d(\mathcal{L}+1)}$ wavelets satisfying $|\mathbf{l}| \leq \mathcal{L}$, but only $2^{\mathcal{L}-1}(\mathcal{L} + 3)$ and $2^{\mathcal{L}-2}(\mathcal{L}^2 + 9\mathcal{L} + 16)$ satisfying $\|\mathbf{l}\|_1 \leq \mathcal{L}$ in 2D and 3D respectively. To fix ideas, we show a schematic of our sampling choices for the coefficients of \dot{W} in figure 3b.

Let $V_H = \text{span}(\psi_1, \dots, \psi_{N_{\mathcal{L}}})$ be the space of piecewise constant functions over the cells \square_k of the Haar mesh $D_{\mathcal{L}}$. In a moment, we will prove that $\dot{W}_{\mathcal{L}} \in V_H$ almost surely and that therefore it can be expressed in terms of the basis functions of V_H as $\dot{W}_{\mathcal{L}} = \sum_{k=1}^{N_{\mathcal{L}}} w_k \psi_k$, where w_k is the value of $\dot{W}_{\mathcal{L}}$ over the Haar cell \square_k . In practice, rather than

computing the inner products of each Haar wavelet with the basis functions of V_h , it is more straightforward to just compute each w_k from the $\mathbf{z}_{\mathcal{L}}$ sample and compute each entry of $\mathbf{b}_{\mathcal{L}}$ as $(\mathbf{b}_{\mathcal{L}})_i = w_{\kappa(i)} \int_D \phi_i \, d\mathbf{x}$, where $\kappa(i)$ is the index k of the Haar cell that contains the support of ϕ_i . Before explaining how this is done in practice, we prove that $\dot{\mathbf{W}}_{\mathcal{L}}$ can be interpreted as the projection of white noise onto V_H and therefore $\dot{\mathbf{W}}_{\mathcal{L}}$ does indeed belong to V_H .

Lemma 4.1. *Let $V_H = \text{span}(\psi_1, \dots, \psi_{N_{\mathcal{L}}})$ be the space of piecewise constant functions over the cells \square_i of the Haar mesh $D_{\mathcal{L}}$. Let P_H be the L^2 projection onto V_H and define the projected white noise $P_H \dot{\mathbf{W}}$ as follows,*

$$(P_H \dot{\mathbf{W}}, v) := \langle \dot{\mathbf{W}}, P_H v \rangle, \quad \forall v \in L^2(D). \quad (19)$$

We then have that $\dot{\mathbf{W}}_{\mathcal{L}} \equiv P_H \dot{\mathbf{W}}$ in $L^2(\Omega, L^2(D))$.

Proof. We note that all the Haar wavelets in the expansion for $\dot{\mathbf{W}}_{\mathcal{L}}$ can be represented as a linear combination of basis functions of V_H . Since there are exactly as many wavelets as basis functions of V_H (see definition 4.1) and since these wavelets are linearly independent, we conclude that the Haar wavelets form a basis of V_H . Therefore $\dot{\mathbf{W}}_{\mathcal{L}} \in L^2(\Omega, V_H)$ and $\langle \dot{\mathbf{W}}_R, v \rangle = 0$ for all $v \in V_H$. Furthermore, for all $v \in L^2(D)$,

$$(\dot{\mathbf{W}}_{\mathcal{L}}, v) = (\dot{\mathbf{W}}_{\mathcal{L}}, P_H v + v^\perp) = (\dot{\mathbf{W}}_{\mathcal{L}}, P_H v) \quad (20)$$

$$= \langle \dot{\mathbf{W}} - \dot{\mathbf{W}}_R, P_H v \rangle = \langle \dot{\mathbf{W}}, P_H v \rangle =: (P_H \dot{\mathbf{W}}, v), \quad (21)$$

almost surely since $\langle \dot{\mathbf{W}}_R, P_H v \rangle = 0$ for all $v \in L^2(D)$. Here we used the fact that all $v \in L^2(D)$ can be split as $v = P_H v + v^\perp$, where $v^\perp \in V_H^\perp$. \square

We now propose the following algorithm for sampling $\dot{\mathbf{W}}_{\mathcal{L}}$:

Algorithm for the sampling of $\dot{\mathbf{W}}_{\mathcal{L}}$:

1. Compute the supermesh between the FEM mesh and the Haar mesh and split the support of the basis functions of V_h to obtain $\{\phi_i\}_{i=1}^m$ each of which with support entirely contained within a single Haar cell. Compute the scalar map $\kappa(i)$ that maps each i to the index k of the Haar cell \square_k that contains the support of ϕ_i and compute $\int_D \phi_i \, d\mathbf{x}$ for all $i = 1, \dots, m$. This step can be done offline.
2. Sample the vector $\mathbf{z}_{\mathcal{L}} \in \mathbb{R}^{N_{\mathcal{L}}}$ of the coefficients in the expression (14) for $\dot{\mathbf{W}}_{\mathcal{L}}$ as $\mathbf{z}_{\mathcal{L}} = [\mathbf{z}_{\text{QMC}}^T, \mathbf{z}_{\text{MC}}^T]^T$, where \mathbf{z}_{QMC} is a randomized low-discrepancy sequence point of dimension equal to the number of coefficients with $\|\mathbf{l}\|_1 \leq \mathcal{L}$ and \mathbf{z}_{MC} is sampled with a pseudo-random number generator.
3. Sample the values w_k of $\dot{\mathbf{W}}_{\mathcal{L}}$ over each Haar mesh cell \square_k as follows. Let $J(\mathbf{l}, \mathbf{n})$ be the index map that given (\mathbf{l}, \mathbf{n}) returns the index j such that $z_{\mathbf{l}, \mathbf{n}} = (\mathbf{z}_{\mathcal{L}})_j$ (the two vectors are the same up to reordering) and define $\mathbf{m}_k \in \mathbb{R}^d$ to be the coordinate vector of the midpoint of \square_k . For each $k = 1, \dots, N_{\mathcal{L}}$ and \mathbf{l} with $\|\mathbf{l}\| \leq \mathcal{L}$, there is only one wavelet with level vector \mathbf{l} with non-zero support over \square_k . For $i = 1, \dots, d$, its wavelet

number is given by $(\bar{\mathbf{n}}_k(\mathbf{l}))_i = \lfloor (\mathbf{m}_k)_i 2^{l_i} \rfloor$ and its sign over \square_k by $\bar{s}_k(\mathbf{l}) = \prod_{i=1}^d s_k(\mathbf{l}_i)$, where the $s_k(\mathbf{l}_i)$ are the signs of the 1D Haar wavelets in the tensor product for $H_{\mathbf{l}, \bar{\mathbf{n}}_k(\mathbf{l})}$, namely

$$s_k(\mathbf{l}_i) = 1 - 2(\lfloor (\mathbf{m}_k)_i 2^{l_i+1} \rfloor \pmod{2}). \quad (22)$$

This expression comes from the fact that Haar wavelets are positive on even Haar cells and negative on odd cells. We set for all $k = 1, \dots, N_{\mathcal{L}}$,

$$w_k = \sum_{\mathbf{l}=0}^{|\mathbf{l}| \leq \mathcal{L}} \bar{s}_k(\mathbf{l}) \mathbf{z}_{J(\mathbf{l}, \bar{\mathbf{n}}_k(\mathbf{l}))} 2^{||\mathbf{l}^+||_1/2} \quad (23)$$

4. For all $i = 1, \dots, m$, set $(\mathbf{b}_{\mathcal{L}})_i = w_{\kappa(i)} \int_D \phi_i \, d\mathbf{x}$.

Remark 4.2. In point 1 and 3 above we exploit the fact that the Haar mesh is uniform and structured. For instance, we can readily obtain the Haar mesh cell in which any point $\mathbf{p} \in D$ lies: it belongs to the $\lfloor (\mathbf{p})_i 2^{\mathcal{L}+1} \rfloor$ -th Haar cell from the origin in the i -th coordinate direction. When supermeshing this makes the search for candidate intersections [21] inexpensive as we always know for a given cell of D_h exactly with which Haar cells it intersects. The expressions for $\bar{\mathbf{n}}_k(\mathbf{l})$ and $\bar{s}_k(\mathbf{l})$ in point 3 above also derive from the same considerations.

Remark 4.3 (Complexity of the sampling of $\dot{W}_{\mathcal{L}}$). Let m be the number of basis functions that span V_h , let $N_{\mathcal{L}} = 2^{d(\mathcal{L}+1)}$ be the number of cells in the Haar mesh and let $N_{\mathcal{L}} = (\mathcal{L} + 2)^d$ be the number of wavelets that are non-zero over a given Haar cell. In general, it is possible to sample $\dot{W}_{\mathcal{L}}$ in $O(m + N_{\mathcal{L}}N_{\mathcal{L}})$ complexity, which reduces to $O(m + N_{\mathcal{L}})$ in the case in which we are using non-standard Haar wavelets⁴ (cf. remark 3.1). If D_h is not nested within $D_{\mathcal{L}}$ a supermesh construction is needed (cf. remark 4.1). In this case the cost complexity becomes $O(N_S m_e + N_{\mathcal{L}}N_{\mathcal{L}})$, where N_S is the number of cells in the supermesh between D_h and $D_{\mathcal{L}}$ and m_e is the number of degrees of freedom on each supermesh cell e . Owing to theorem 1.1 in [12], when D_h is quasi-uniform we have $N_S = O(N_h + N_{\mathcal{L}})$, where N_h is the number of cells of D_h and $a > 0$. This gives a linear cost complexity in the number of cells of D_h and log-linear in the number of cells of $D_{\mathcal{L}}$ since $N_{\mathcal{L}} = O((\log_2(N_{\mathcal{L}})/d)^d)$. The log-term can be dropped if we use non-standard wavelets.

4.2 Sampling of \dot{W}_R

We now consider the efficient sampling of \dot{W}_R . Dealing with an infinite summation is complicated. However, we can circumvent this problem by noting that the covariance of \dot{W}_R is known since, as $\dot{W}_{\mathcal{L}}$ is independent from \dot{W}_R by construction, for all $u, v \in L^2(D)$ we have

$$\mathbb{E}[\langle \dot{W}_R, u \rangle \langle \dot{W}_R, v \rangle] = \mathbb{E}[\langle \dot{W}, u \rangle \langle \dot{W}, v \rangle] - \mathbb{E}[\langle \dot{W}_{\mathcal{L}}, u \rangle \langle \dot{W}_{\mathcal{L}}, v \rangle], \quad (24)$$

where the covariance of \dot{W} is known by definition 2.1 and the covariance of $\dot{W}_{\mathcal{L}}$ is given by the following lemma.

⁴In this case it is possible to use a multi-dimensional generalization of the Brownian bridge construction (of which $\dot{W}_{\mathcal{L}}$ is the derivative) which is well known in the computational finance literature [27].

Lemma 4.2. Let \square_i for $i = 1, \dots, N_{\mathcal{L}}$ be the i -th cell of $D_{\mathcal{L}}$ of volume $|\square_i| = 2^{d(\mathcal{L}+1)} = |\square_H|$ for all i (see definition 4.1). Then, for all $u, v \in L^2(D)$,

$$\mathcal{C}_{\mathcal{L}}(u, v) = \mathbb{E}[(\dot{W}_{\mathcal{L}}, u)(\dot{W}_{\mathcal{L}}, v)] = \sum_{i=1}^{N_{\mathcal{L}}} \frac{1}{|\square_i|} \int_{\square_i} u \, d\mathbf{x} \int_{\square_i} v \, d\mathbf{x}. \quad (25)$$

Proof. Let P_H be the L^2 projection onto V_H , then for all $u \in L^2(D)$ we have that $P_H u = \sum_{i=1}^{N_{\mathcal{L}}} u_i \psi_i$ satisfies

$$(P_H u, v_H) = (u, v_H), \quad \forall v_H \in V_H. \quad (26)$$

A standard FEM calculation gives that the coefficients u_i are given by

$$u_i = \frac{1}{|\square_i|} (u, \psi_i) = \frac{1}{|\square_i|} \int_{\square_i} u \, d\mathbf{x}. \quad (27)$$

We conclude by using lemma 4.1 to show that, for all $u, v \in V$ such that $P_H u = \sum_{i=1}^{N_{\mathcal{L}}} u_i \psi_i$ and $P_H v = \sum_{i=1}^{N_{\mathcal{L}}} v_i \psi_i$,

$$\begin{aligned} \mathbb{E}[(\dot{W}_{\mathcal{L}}, u)(\dot{W}_{\mathcal{L}}, v)] &= \mathbb{E}[\langle \dot{W}, P_H u \rangle \langle \dot{W}, P_H v \rangle] = (P_H u, P_H v) \\ &= \sum_{i,j=1}^{N_{\mathcal{L}}} u_i v_j (\psi_i, \psi_j) = \sum_{i=1}^{N_{\mathcal{L}}} |\square_i| u_i v_i = \sum_{i=1}^{N_{\mathcal{L}}} \frac{1}{|\square_i|} \int_{\square_i} u \, d\mathbf{x} \int_{\square_i} v \, d\mathbf{x}. \end{aligned} \quad (28)$$

Note that a similar procedure also yields an expression for the pointwise covariance of $\dot{W}_{\mathcal{L}}$. Let $\dot{W}_{\mathcal{L}} = \sum_{k=1}^{N_{\mathcal{L}}} w_k \psi_k$ be the representation of $\dot{W}_{\mathcal{L}}$ in terms of the basis functions of V_H , then, for all $\mathbf{x} \in \square_i, \mathbf{y} \in \square_j$, we have

$$\mathbb{E}[\dot{W}_{\mathcal{L}}(\mathbf{x}) \dot{W}_{\mathcal{L}}(\mathbf{y})] = \delta_{ij} \mathbb{E}[w_i w_j] = \delta_{ij} \frac{1}{|\square_i|^2} \mathbb{E}[(\langle \dot{W}, \psi_i \rangle)^2] = \frac{\delta_{ij}}{|\square_i|}. \quad (29)$$

Here by δ_{ij} we denote the Kronecker delta and we used equation (27) in the second step. \square

It is then readily shown from lemma 4.2 and from (24) that the covariance of \dot{W}_R is

$$\mathcal{C}_R(u, v) = \mathbb{E}[\langle \dot{W}_R, u \rangle \langle \dot{W}_R, v \rangle] = (u, v) - \sum_{i=1}^{N_{\mathcal{L}}} \frac{1}{|\square_i|} \int_{\square_i} u \, d\mathbf{x} \int_{\square_i} v \, d\mathbf{x}, \quad (30)$$

for all $u, v \in L^2(D)$. From lemma 4.2 and from definition 2.1 we deduce that if the supports of u and v never share the same Haar mesh cell, then

$$\mathbb{E}[(\dot{W}_{\mathcal{L}}, u)(\dot{W}_{\mathcal{L}}, v)] = \mathbb{E}[\langle \dot{W}, u \rangle \langle \dot{W}, v \rangle] = \mathbb{E}[\langle \dot{W}_R, u \rangle \langle \dot{W}_R, v \rangle] = 0, \quad (31)$$

i.e. the action of $\dot{W}_{\mathcal{L}}$ is exactly the same as the action of white noise in this case and the correction term \dot{W}_R is not needed. This means that the restrictions of $\dot{W}_{\mathcal{L}}$ and \dot{W}_R to separate Haar mesh cells are statistically independent from each other. Thanks to this property, we can consider each Haar cell separately and only account for the correlations among the pairings of \dot{W}_R with test functions that belong to the same cell. Since the computations on separate Haar cells are independent, these operations can be performed simultaneously in parallel.

Before proceeding, we show that \mathcal{C}_R is a proper covariance function, i.e. that it is positive semi-definite.

Lemma 4.3. *The covariance of \dot{W}_R , \mathcal{C}_R , is positive semi-definite.*

Proof. With the same notation as in the proof of lemma 4.2, we have that, for all $u \in L^2(D)$,

$$\mathcal{C}_R(u, u) = \mathbb{E}[(\langle \dot{W}_R, u \rangle)^2] = \mathbb{E}[(\langle \dot{W} - P_H \dot{W}, u \rangle)^2] = \mathbb{E}[(\langle \dot{W}, u - P_H u \rangle)^2] = \|u - P_H u\|_{L^2(D)}^2, \quad (32)$$

since $\dot{W}_R = \dot{W} - \dot{W}_\mathcal{L} = \dot{W} - P_H \dot{W}$. Hence $\mathcal{C}_R(u, u)$ is always non-negative and it is zero if and only if $u \in V_H$. \square

Remark 4.4. From the proofs of lemmas 4.2 and 4.3, we see that we can interpret $\dot{W}_\mathcal{L}$ as the L^2 -projection of white noise onto V_H . In principle, if $D_\mathcal{L}$ is fine enough (or if $V_h \equiv V_H$), the correction \dot{W}_R is not needed at all. However, Haar wavelets are only piecewise constant and we might only expect first order convergence of $\dot{W}_\mathcal{L}$ to \dot{W} . If so, large QMC dimensions and an extremely fine Haar mesh would be needed to make the correction term \dot{W}_R negligible and this translates into very expensive samples of $\dot{W}_\mathcal{L}$.

The sampling of \dot{W}_R can be performed independently on each Haar cell. If we focus our attention only on the basis functions $\phi_1, \dots, \phi_{m_k} \in V_h$ of support entirely contained within a given Haar cell \square_k , we note that the expression (30) for \mathcal{C}_R simplifies to

$$\mathcal{C}_R(\phi_i, \phi_j) = (\phi_i, \phi_j) - \frac{1}{|\square_k|} \int_{\square_k} \phi_i \, d\mathbf{x} \int_{\square_k} \phi_j \, d\mathbf{x}, \quad \text{for all } i, j \in \{1, \dots, m_k\}. \quad (33)$$

Similarly as in [13], the sampling of \dot{W}_R over \square_k boils down to sampling a zero-mean Gaussian vector \mathbf{b}_R^k with entries $(\mathbf{b}_R^k)_i = \langle \dot{W}_R, \phi_i \rangle$ and covariance matrix C_R^k of entries $(C_R^k)_{ij}$ given by

$$\mathbf{b}_R^k \sim \mathcal{N}(0, C_R^k), \quad (C_R^k)_{ij} = \mathcal{C}_R(\phi_i, \phi_j). \quad (34)$$

If we let M_k be the local mass matrix over the space spanned by the $\{\phi_i\}_{i=1}^{m_k}$, with entries $(M_k)_{ij} = (\phi_i, \phi_j)$ and if we let the vector $\mathbf{I}^k \in \mathbb{R}^{m_k}$ be given by

$$\mathbf{I}^k = \left[\int_{\square_k} \phi_1 \, d\mathbf{x}, \dots, \int_{\square_k} \phi_{m_k} \, d\mathbf{x} \right]^T, \quad (35)$$

we can write C_R^k as

$$C_R^k = M_k - \frac{1}{|\square_k|} \mathbf{I}^k (\mathbf{I}^k)^T. \quad (36)$$

Note that a consequence of lemma 4.3 is that C_R^k is positive semi-definite with null-space spanned by the vector $\mathbf{1} \in \mathbb{R}^{m_k}$, the length m_k vector of all ones (piecewise constant functions over $D_\mathcal{L}$ are in the null-space of the covariance). The sampling of a Gaussian vector with this covariance through factorization is expensive as direct factorization of C_R^k (e.g. Cholesky) has an $O(m_k^3)$ and $O(m_k^2)$ cost and memory complexity respectively and it is therefore to be avoided.

We now show how \mathbf{b}_R^k can be sampled efficiently by extending the techniques presented in [13]. The main idea is to first sample a Gaussian vector with covariance M_k in linear

complexity and then perform an efficient update to obtain a sample of \mathbf{b}_R^k . We can write the action of \dot{W}_R against each ϕ_i as

$$\langle \dot{W}_R, \phi_i \rangle = \langle \dot{W} - \dot{W}_{\mathcal{L}}, \phi_i \rangle = \langle \dot{W}, \phi_i \rangle - \langle \dot{W}_{\mathcal{L}}, \phi_i \rangle = (\mathbf{b}_M^k)_i - w_k (\mathbf{I}^k)_i, \quad (37)$$

where \mathbf{I}^k is given by (35), w_k by

$$w_k = \frac{1}{|\square_k|} \langle \dot{W}, \mathbf{1}_{\square_k} \rangle, \quad w_k \sim \mathcal{N} \left(0, \frac{1}{|\square_k|} \right), \quad (38)$$

and the vector $\mathbf{b}_M^k \in \mathbb{R}^{m_k}$ is given entrywise by

$$(\mathbf{b}_M^k)_i = \langle \dot{W}, \phi_i \rangle, \quad i = 1, \dots, m_k. \quad (39)$$

The variables w_k and \mathbf{b}_M^k are by definition 2.1 all zero-mean joint Gaussian variables with covariance

$$\mathbb{E}[w_k w_k] = \frac{1}{|\square_k|}, \quad \mathbb{E}[\mathbf{b}_M^k w_k] = \frac{\mathbf{I}^k}{|\square_k|}, \quad \mathbb{E}[\mathbf{b}_M^k (\mathbf{b}_M^k)^T] = M_k. \quad (40)$$

Thanks to these relations and to (37), if we set

$$\mathbf{b}_R^k = \mathbf{b}_M^k - w_k \mathbf{I}^k, \quad (41)$$

then the covariance of \mathbf{b}_R^k is correct (cf. equation (36)) since

$$\begin{aligned} \mathbb{E}[\mathbf{b}_R^k (\mathbf{b}_R^k)^T] &= \mathbb{E}[(\mathbf{b}_M^k - w_k \mathbf{I}^k)(\mathbf{b}_M^k - w_k \mathbf{I}^k)^T] \\ &= \mathbb{E}[\mathbf{b}_M^k (\mathbf{b}_M^k)^T] - \mathbb{E}[\mathbf{b}_M^k w_k] (\mathbf{I}^k)^T - \mathbf{I}^k \mathbb{E}[w_k \mathbf{b}_M^k]^T + \mathbb{E}[w_k w_k] \mathbf{I}^k (\mathbf{I}^k)^T \\ &= M_k - \frac{1}{|\square_k|} \mathbf{I}^k (\mathbf{I}^k)^T. \end{aligned} \quad (42)$$

In what follows, we exploit the fact that constants can be represented exactly by the FEM subspace V_h , i.e. $c \in V_h$ for all $c \in \mathbb{R}$. This assumption is standard and it is required to achieve FEM convergence by the Bramble-Hilbert lemma, cf. lemma 4.3.8 in [7]. Let $\phi_k = [\phi_1, \dots, \phi_{m_k}]^T$. This means that for each Haar cell \square_k there exists a vector $\mathbf{c}_k \in \mathbb{R}^{m_k}$ such that $\mathbf{1}_{\square_k} \equiv \mathbf{c}_k \cdot \phi_k$. It is then straightforward to obtain w_k from \mathbf{b}_M^k since

$$\mathbf{c}_k \cdot \mathbf{b}_M^k = \sum_{i=1}^{m_k} \langle \dot{W}, (c_k)_i \phi_i \rangle = \langle \dot{W}, \mathbf{c}_k \cdot \phi_k \rangle = \langle \dot{W}, \mathbf{1}_{\square_k} \rangle = |\square_k| w_k, \quad (43)$$

hence $w_k = |\square_k|^{-1} \mathbf{c}_k \cdot \mathbf{b}_M^k$. Note that \mathbf{c}_k is always known, e.g. for Lagrange basis functions on simplices we have $\mathbf{c}_k = \mathbf{1} \in \mathbb{R}^{m_k}$.

We can now sample \dot{W}_R from its distribution by using the following algorithm, in which we exploit the same strategy we presented in [13]:

Algorithm for the efficient sampling of \dot{W}_R .

1. Loop over each Haar cell \square_k .
2. Use the technique presented in section 4.1 of [13] to work supermesh cell by supermesh cell and sample a Gaussian vector $\mathbf{b}_M^k \sim \mathcal{N}(0, M_k)$ in linear cost complexity.
3. Set $w_k = |\square_k|^{-1} \mathbf{c}_k \cdot \mathbf{b}_M^k$ and compute $\mathbf{b}_R^k = \mathbf{b}_M^k - w_k \mathbf{I}^k$.

Remark 4.5. The sampling strategies for $\dot{W}_\mathcal{L}$ and \dot{W}_R presented in this work are conceptually different. In the $\dot{W}_\mathcal{L}$ case we use the Haar wavelet representation to make sure that the variables in the quasi-random sequence are ordered correctly. Therefore the use of the Haar representation is crucial in the sampling of $\dot{W}_\mathcal{L}$. In the \dot{W}_R case, instead, the ordering is irrelevant as \dot{W}_R is sampled by using pseudo-random numbers. For this reason we can “forget” about the wavelet representation in this case and sample \dot{W}_R as it is done for any standard Gaussian field, i.e. by factorising its covariance matrix after discretization.

Remark 4.6. This algorithm has $O(\mathcal{N}_\mathcal{S} m_e^3)$ cost and $O(\mathcal{N}_\mathcal{S} m_e^2)$ memory complexity, where $\mathcal{N}_\mathcal{S}$ is the total number of supermesh cells [13]. As discussed in remark 4.3, $\mathcal{N}_\mathcal{S}$ is of $O(\mathcal{N}_h + \mathcal{N}_\mathcal{L})$, where \mathcal{N}_h and $\mathcal{N}_\mathcal{L}$ are the number of cells of D_h and of $D_\mathcal{L}$ respectively.

5 Sampling coupled realizations for MLQMC

We now generalize the QMC sampling algorithm just presented to the MLQMC case. Compared to standard Monte Carlo, both MLMC and QMC already bring a significant computational improvement. When the two are combined into MLQMC, it is sometimes possible to obtain the best of both worlds and further improve the computational complexity and speed. However, to do so, we must be able to satisfy the requirements and assumptions underlying both QMC and MLMC: we must order the dimensions of our random input in decaying order of importance as in QMC and introduce an approximation level hierarchy and enforce a good coupling between the levels as in MLMC. We now show how this can be done with white noise sampling.

In what follows we assume we have a MLQMC hierarchy of possibly non-nested FEM approximation subspaces $\{V^\ell\}_{\ell=1}^L$ over the meshes $\{D_h^\ell\}_{\ell=1}^L$ and of accuracy increasing with ℓ . Since as in the MLMC case (see [13]) the only stochastic element in (15) is white noise, on each MLQMC level we must be able to draw Matérn field samples $u_\ell \in V^\ell$ and $u_{\ell-1} \in V^{\ell-1}$ for $\ell > 1$ that satisfy the following variational problems coupled by the same white noise sample: for a given $\omega_\ell^n \in \Omega$, find $u_\ell \in V^\ell$ and $u_{\ell-1} \in V^{\ell-1}$ such that

$$(u_\ell, v_\ell) + \kappa^{-2}(\nabla u_\ell, \nabla v_\ell) = \langle \dot{W}, v_\ell \rangle(\omega_\ell^n), \quad \text{for all } v_\ell \in V^\ell, \quad (44)$$

$$(u_{\ell-1}, v_{\ell-1}) + \kappa^{-2}(\nabla u_{\ell-1}, \nabla v_{\ell-1}) = \langle \dot{W}, v_{\ell-1} \rangle(\omega_\ell^n), \quad \text{for all } v_{\ell-1} \in V^{\ell-1}. \quad (45)$$

where the terms on the right hand side are coupled in the sense that they are centred Gaussian random variables with covariance $\mathbb{E}[\langle \dot{W}, v_t \rangle \langle \dot{W}, v_s \rangle] = (v_t, v_s)$ for $t, s \in \{\ell, \ell-1\}$, as given by definition 2.1. Again we order the dimensions of white noise by expanding it in the Haar wavelet basis as in (13), but this time we allow the Haar level to possibly increase

with the MLQMC level and we split the expansion at the finer Haar level between the two MLQMC levels, \mathcal{L}_ℓ ,

$$\dot{W} = \dot{W}_{\mathcal{L}_\ell} + \dot{W}_{R_\ell}, \quad (46)$$

where the splitting of the expansion is done in the same way as in equation (14). From now on we assume that $\mathcal{L}_{\ell-1} \leq \mathcal{L}_\ell$, although extending the methods presented to decreasing Haar level hierarchies is straightforward. Let $\{\phi_i^\ell\}_{i=1}^{m_\ell}$ and $\{\phi_j^{\ell-1}\}_{j=1}^{m_{\ell-1}}$ be the basis functions spanning V^ℓ and $V^{\ell-1}$ respectively. Sampling white noise on both MLQMC levels again means to sample the vectors $\mathbf{b}_{\mathcal{L}}^\ell$, $\mathbf{b}_{\mathcal{L}}^{\ell-1}$, \mathbf{b}_R^ℓ and $\mathbf{b}_R^{\ell-1}$, with entries given by,

$$(\mathbf{b}_{\mathcal{L}}^t)_i = \langle \dot{W}_{\mathcal{L}_\ell}, \phi_i^t \rangle, \quad (\mathbf{b}_R^t)_i = \langle \dot{W}_{R_\ell}, \phi_i^t \rangle, \quad \text{for } i = 1, \dots, m_t, \quad t \in \{\ell, \ell-1\}. \quad (47)$$

Since we both require a multilevel coupling and a Haar wavelet expansion, this time we need to construct a *three-way* supermesh S_h between $D_{\mathcal{L}_\ell}$, D_h^ℓ and $D_h^{\ell-1}$ (note that $D_{\mathcal{L}_{\ell-1}}$ is always nested within $D_{\mathcal{L}_\ell}$ so there is no need for a four-way supermesh). Thanks to the supermesh construction we can split the support of all the basis functions so that each ϕ_i^ℓ and $\phi_j^{\ell-1}$ has support entirely contained within a single Haar cell. In fact, we will assume for simplicity from now on that the supports of all basis functions have this property. The sampling of \dot{W} in the MLQMC case is extremely similar to that of the QMC case with only a few differences concerning the sampling of \dot{W}_{R_ℓ} which we will now highlight.

Again, portions of \dot{W}_{R_ℓ} on separate Haar cells of $D_{\mathcal{L}_\ell}$ are independent and we can therefore sample \dot{W}_{R_ℓ} Haar cell-wise. For each Haar cell \square_k and for $t \in \{\ell, \ell-1\}$, let $\phi_1^t, \dots, \phi_{m_k^t}^t$ be the basis functions with non-zero support over \square_k and define the Haar cell correction vectors $\mathbf{b}_{R,k}^t$ with entries $(\mathbf{b}_{R,k}^t)_i = \langle \dot{W}, \phi_i^t \rangle$ for $i \in \{1, \dots, m_k^t\}$ and covariances given by,

$$\mathbb{E}[\mathbf{b}_{R,k}^t (\mathbf{b}_{R,k}^t)^T] = M_k^t - \frac{1}{|\square_k|} \mathbf{I}_t^k (\mathbf{I}_t^k)^T, \quad \mathbb{E}[\mathbf{b}_{R,k}^\ell (\mathbf{b}_{R,k}^{\ell-1})^T] = M_k^{\ell, \ell-1} - \frac{1}{|\square_k|} \mathbf{I}_\ell^k (\mathbf{I}_{\ell-1}^k)^T, \quad (48)$$

where $(M_k^t)_{ij} = (\phi_i^t, \phi_j^t)$, $(M_k^{\ell, \ell-1})_{ij} = (\phi_i^\ell, \phi_j^{\ell-1})$ and $(\mathbf{I}_t^k)_i = \int_D \phi_i^t d\mathbf{x}$. If we define w_k as in (38) we can again write

$$\mathbf{b}_{R,k}^t = \mathbf{b}_{M,k}^t - w_k \mathbf{I}_t^k, \quad \text{for } t \in \{\ell, \ell-1\}, \quad (49)$$

where $\mathbf{b}_{M,k}^t \sim \mathcal{N}(0, M_k^t)$. Since constants can be represented exactly by both V^ℓ and $V^{\ell-1}$, i.e. for all $c \in \mathbb{R}$ and for all $t \in \{\ell, \ell-1\}$, we have that $c \in V^t$, then there exist two vectors \mathbf{c}_k^ℓ and $\mathbf{c}_k^{\ell-1}$ such that $\mathbb{1}_{\square_k} \equiv \mathbf{c}_k^\ell \cdot \phi_k^\ell \equiv \mathbf{c}_k^{\ell-1} \cdot \phi_k^{\ell-1}$, where $\phi_k^t = [\phi_1^t, \dots, \phi_{m_k^t}^t]^T$ for $t \in \{\ell, \ell-1\}$. The same argument used to derive equation (43) then gives

$$w_k = \frac{1}{|\square_k|} \mathbf{c}_k^\ell \cdot \mathbf{b}_{M,k}^\ell = \frac{1}{|\square_k|} \mathbf{c}_k^{\ell-1} \cdot \mathbf{b}_{M,k}^{\ell-1}. \quad (50)$$

We can now proceed with the coupled sampling of \dot{W} for MLQMC as follows:

Algorithm for the efficient sampling of \dot{W} for MLQMC

1. Compute the three-way supermesh between the FEM meshes and the Haar mesh $D_{\mathcal{L}_\ell}$ and split the support of the basis functions of V^ℓ and $V^{\ell-1}$ to obtain $\{\phi_i^t\}_{i=1}^{m^t}$ for $t \in \{\ell, \ell-1\}$ each of which with support entirely contained within a single Haar cell. Compute the scalar maps $\kappa^t(i)$ that map each i to the index k of the Haar cell \square_k that contains the support of ϕ_i^t and compute $\int_D \phi_i^t d\mathbf{x}$ for all $i = 1, \dots, m^t$ and for $t \in \{\ell, \ell-1\}$. This step can be done offline.
2. Let $\mathcal{N}_{\mathcal{L}_\ell}$ be the number of cells of $D_{\mathcal{L}_\ell}$. Sample the vector $\mathbf{z}_{\mathcal{L}_\ell} \in \mathbb{R}^{\mathcal{N}_{\mathcal{L}_\ell}}$ of the coefficients in the expression for $\dot{W}_{\mathcal{L}_\ell}$ as $\mathbf{z}_{\mathcal{L}_\ell} = [\mathbf{z}_{\text{QMC}}^T, \mathbf{z}_{\text{MC}}^T]^T$, where \mathbf{z}_{QMC} is a randomized low-discrepancy sequence point of dimension equal to the number of coefficients with $\|\mathbf{l}\|_1 \leq \mathcal{L}_\ell$ and \mathbf{z}_{MC} is sampled with a pseudo-random number generator.
3. Compute the Haar cell values \bar{w}_k of $\dot{W}_{\mathcal{L}_\ell}$ over all \square_k for $k = 1, \dots, \mathcal{N}_{\mathcal{L}_\ell}$ in the same way as in the QMC case (this step does not depend on the FEM meshes).
4. Use the technique presented in section 4.2 of [13] to work supermesh cell by supermesh cell and sample in linear cost complexity the coupled Gaussian vectors $\mathbf{b}_{M,k}^\ell$ and $\mathbf{b}_{M,k}^{\ell-1}$ with covariance,

$$\left[\frac{\mathbf{b}_{M,k}^\ell}{\mathbf{b}_{M,k}^{\ell-1}} \right] = \left[\frac{M_k^\ell}{(M_k^{\ell,\ell-1})^T} \middle| \frac{M_k^{\ell,\ell-1}}{M_k^{\ell-1}} \right]. \quad (51)$$

5. For all $t \in \{\ell, \ell-1\}$, compute $(\mathbf{b}_{\mathcal{L}_\ell}^t)_i = \bar{w}_{\kappa^t(i)} \int_D \phi_i^t d\mathbf{x}$ for all $i = 1, \dots, m^t$, then set $w_k = |\square_k|^{-1} \mathbf{c}_k^{\ell-1} \cdot \mathbf{b}_{M,k}^{\ell-1}$ and compute $\mathbf{b}_{R,k}^t = \mathbf{b}_{M,k}^t - w_k \mathbf{I}_t^k$.

Remark 5.1 (Complexity of the sampling of \dot{W} for MLQMC). The overall complexity of this sampling strategy is $O(\mathcal{N}_S m_\ell + \mathcal{N}_{\mathcal{L}_\ell} \mathcal{N}_{\mathcal{L}_\ell})$ in the standard Haar wavelet case and $O(\mathcal{N}_{S_\ell} m_\ell + \mathcal{N}_{\mathcal{L}_\ell})$ in the non-standard case (cf. remark 3.1), where (cf. remark 4.3) \mathcal{N}_{S_ℓ} is the number of cells of the three-way supermesh on the MLQMC level ℓ , m_ℓ is the number of dofs of V^ℓ per cell of D_h^ℓ and $\mathcal{N}_{\mathcal{L}_\ell}$ is the number of wavelets that have non-zero support over any of the $\mathcal{N}_{\mathcal{L}_\ell}$ cells of $D_{\mathcal{L}_\ell}$. Since $\mathcal{N}_{S_\ell} = O(\mathcal{N}_h^\ell + \mathcal{N}_{\mathcal{L}_\ell})$ (cf. theorem 1.1 in [12]), where \mathcal{N}_h^ℓ is the number of cells of D_h^ℓ , this gives an overall linear cost complexity in \mathcal{N}_h^ℓ and log-linear (linear for non-standard wavelets) in $\mathcal{N}_{\mathcal{L}_\ell}$.

Remark 5.2 (Simpler cases: nested meshes and p -refinement). When the MLQMC mesh hierarchy is nested and/or the hierarchy is composed by taking a single mesh and increasing the polynomial degree of the FEM subspaces we have $V^{\ell-1} \subseteq V^\ell$. In this case everything we discussed still applies with the following simplifications: only a two-way supermesh between D_h^ℓ and $D_{\mathcal{L}_\ell}$ is needed on each MLQMC level in the h -refinement case. In the p -refinement case we only have one FEM mesh D_h and a single two-way supermesh construction is needed between D_h and the finest Haar mesh $D_{\mathcal{L}_L}$.

Remark 5.3 (Non-nested mesh hierarchies and embedded domains). In practice, we assume that we are given a user-provided hierarchy $\{G_h^\ell\}_{\ell=0}^L$ of possibly non-nested FEM meshes of the domain G on which we need the Matérn field samples. From this we construct a boxed domain D s.t. $G \subset\subset D$ and a corresponding hierarchy of Haar meshes $\{D_{\mathcal{L}_\ell}\}_{\ell=0}^L$ and

of FEM meshes of D , $\{D_h^\ell\}_{\ell=0}^L$. As in [13], it is convenient to construct each D_h^ℓ so that G_h^ℓ is nested within it, so that each Matérn field sample can be transferred exactly and at negligible cost on the mesh on which it is needed (this is the embedded domain strategy proposed in [50]).

Remark 5.4 (Generic wavelets). We expect the generalization of the presented sampling methods to generic wavelets to be straight-forward, although it is unclear as to whether this would bring any considerable advantage. We leave this investigation to future research.

Remark 5.5 (General domains). We briefly speculate on the extension of the methods presented to more general (i.e. non boxed) domains. The same sampling method could be generalized to general convex domains by introducing “generalized” Haar wavelets and meshes, obtained by partitioning a mesh into sub-regions and defining the cells of $D_{\mathcal{L}}$ through aggregation of the cells of D_h . Establishing any theoretical results in this case would be more complex, but the same algorithm should carry forward after accounting for the fact that the “Haar cells” obtained through aggregation would have variable volume. The advantage of doing this is that no supermesh would then be required in the QMC case (the Haar mesh would be nested within D_h by construction) and only one supermesh construction would be needed (between D_h^ℓ and $D_h^{\ell-1}$) in the non-nested MLQMC case. We leave the implementation of this extension to future work.

6 Numerical results

We now test the algorithms presented. We consider test problem (62) over the domain $G = (-0.5, 0.5)^d$ with forcing term $f = 1$, i.e. we solve

$$\begin{aligned} -\nabla \cdot (e^{u(\mathbf{x}, \omega)} \nabla p(\mathbf{x}, \omega)) &= 1, & \mathbf{x} \in G = (-0.5, 0.5)^d, & \omega \in \Omega, \\ p(\mathbf{x}, \omega) &= 0, & \mathbf{x} \in \partial G, & \omega \in \Omega, \end{aligned} \quad (52)$$

where $u(\mathbf{x}, \omega)$ is a Matérn field sampled by solving equation (15) over $D = (-1, 1)^d$ with $\lambda = 0.25$ and mean and standard deviation chosen so that $\mathbb{E}[e^u] = 1$, $\mathbb{V}[e^u] = 0.2$. For simplicity, we take the $L^2(G)$ norm of p squared, $P(\omega) = \|p\|_{L^2(G)}^2(\omega)$ as our output functional of interest.

Remark 6.1. We do not consider functionals of the Matérn field u and we directly focus on the estimation of $\mathbb{E}[P]$. The reason is that in 2D and 3D the smoothness of u is low and we only observe standard Monte Carlo convergence rates in numerical experiments (not shown).

We solve equations (15) and (52) with the FEniCS software package [47]. For simplicity, we consider the h -refinement case and we discretize the equations using continuous piecewise-linear Lagrange elements. We employ the conjugate gradient routine of PETSc [2] preconditioned by the BoomerAMG algebraic multigrid algorithm from Hypre [18] for the linear solver for both equations. We declare convergence when the absolute size of the preconditioned residual norm is below a tolerance of 10^{-12} . We employ the libsupermesh software package [48] for the supermesh constructions. We use random digital shifted Sobol’ sequences sampled with a custom-built⁵ Python and C wrapper of the Intel® Math

⁵Available online at bitbucket.org/croci/mkl_sobol/.

Kernel Library Sobol' sequence implementation augmented with Joe and Kuo's primitive polynomials and direction numbers [37] (maximum dimension = 21201). All the algorithms presented (as well as the MLMC methods from [13]) are available online within the femlmc software package⁶.

We construct the mesh hierarchies $\{G_h^\ell\}_{\ell=0}^L$ and $\{D_h^\ell\}_{\ell=0}^L$ so that, for all MLQMC levels ℓ , G_h^ℓ is nested within D_h^ℓ , yet $G_h^{\ell-1}$ and $D_h^{\ell-1}$ are not nested within G_h^ℓ and D_h^ℓ respectively. We take all the meshes in both hierarchies to be simplicial, uniform and structured for simplicity with mesh sizes $h_\ell = 2^{-(\ell+1)}$ in 1D, $h_\ell = 2^{-1/2} 2^{-\ell}$ in 2D and $h_\ell = \sqrt{3} 2^{-(\ell+1)}$ in 3D, although we do not exploit this structure in the implementation.

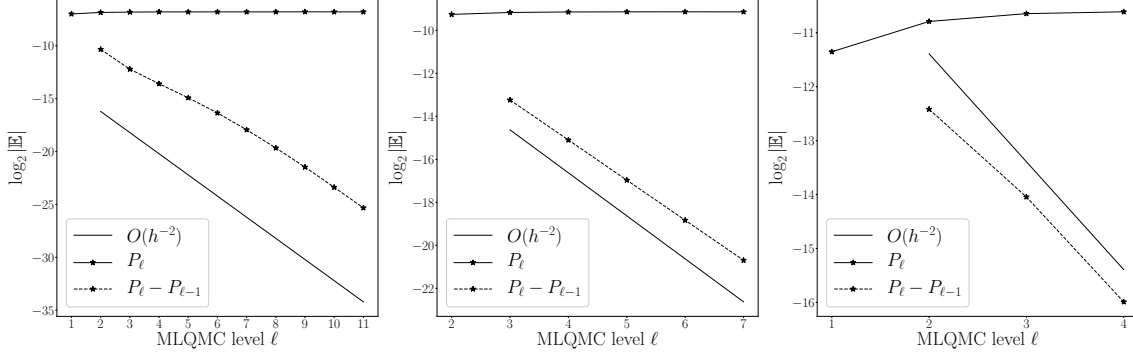


Figure 4: *Logarithm of the absolute value of the expected value of P_ℓ and $P_\ell - P_{\ell-1}$ as a function of the MLQMC level ℓ in 1D (left), 2D (middle) and 3D (right). We observe a decay rate of $O(h^{-2})$ in all dimensions. These results are independent from the Haar level chosen as we always compute the exact action of white noise independently from the choice of \mathcal{L} .*

We first study how the quantities $|\mathbb{E}[P_\ell]|$ and $|\mathbb{E}[P_\ell - P_{\ell-1}]|$ vary as the MLQMC level is increased. Assuming that u can be sampled exactly, we expect the MLMC parameter value α to be $\alpha = \min(\nu + 1, p + 1)$ [30]. Numerical results are shown in figure 4 where we observe a decay rate of $\alpha = 2$ in 1D, 2D and 3D. In 3D we might have expected the rate to be 1.5 due to the lack of smoothness of the coefficient u which is only in $C^{0.5-\epsilon}(\bar{G})$ for any $\epsilon > 0$ [30]. However, at the discrete level, the FEM approximation of u is in $W^{1,\infty}(G)$ a.s. and we might be observing a pre-asymptotic regime.

As a next step, we analyse the convergence behaviour of QMC and MLQMC with respect to the number of samples. In the supplementary material (theorem B.1) we show that in the QMC case we expect an initial faster-than-MC convergence rate followed by a standard MC rate of $O(N^{-1/2})$ and that the higher the Haar level is, the later the transition between the two regimes happens. No results regarding the MLQMC case were derived, but we expect a similar behaviour to occur. Furthermore, we would like to determine whether the multilevel technique can improve on QMC by bringing further variance reduction.

Remark 6.2. Another way of interpreting our hybrid approach is that we are splitting white noise into a smooth part $\tilde{W}_\mathcal{L}$ and a rough part \tilde{W}_R . QMC is effective at reducing the statistical error coming from the smooth part, but performs poorly when approximating the rough part and we are better off with directly using pseudo-random points. This aspect

⁶Available online at bitbucket.org/croci/femlmc/.

was experimentally investigated in [3] and can be seen as another instance of the *effective dimensionality* principle mentioned in section 2.

We draw inspiration from the original MLQMC paper by Giles and Waterhouse [24] and we study the convergence behaviour of both QMC and MLQMC as the MLQMC level is increased. Results are shown in figure 5. We increase the Haar level with the MLQMC level so that the Haar mesh size is always proportional to the FEM mesh size, but we consider two different strategies: 1) we choose the Haar mesh size to be comparable to the FEM mesh size (figures 5a, 5c, 5e) and 2) we pick the Haar mesh size to be smaller than the FEM mesh size (figures 5b, 5d, 5f). For both scenarios, we compute the variance \mathbb{V}_ℓ of the (ML)QMC estimator on MLQMC level ℓ by using $M = 128$ ($M = 64$ in 3D) randomizations of the Sobol' sequence used and we monitor the quantity $\log_2(N_\ell \mathbb{V}_\ell)$ as the number of samples N_ℓ is increased. Various colours are used in figure 5 to indicate the different sample sizes. The horizontal lines correspond to QMC and the oblique lines to MLQMC.

For standard MC and MLMC, we have $\mathbb{V}_\ell = O(N^{-1})$, giving a $\log_2(N_\ell \mathbb{V}_\ell)$ of $O(1)$. For this reason, if we were observing a MC-like convergence rate, we would see the different coloured lines of figure 5 overlapping. The fact that this does not happen means that we are in fact observing a QMC-like rate which is faster than $O(N^{-1})$ (for the variance). However, it is clear by looking at figures 5a, 5c and 5e that as N_ℓ grows the lines get closer to each other, marking a decay to a $O(N^{-1})$ rate of convergence (for the variance) as predicted by theorem B.1 (see supplementary material). By comparing the figures on the left hand side to those on the right hand side, it is also clear that increasing the Haar level delays the occurrence of this behaviour both in the QMC case and in the MLQMC case. Furthermore, it appears that in the MLQMC case the convergence rate decays sooner than in the QMC case. Finally, we note that MLQMC indeed benefits from the combination of QMC and MLMC: the variance of the MLQMC estimator on any level is always smaller than the corresponding QMC estimator for the same number of samples, with large variance reductions on the fine levels.

We now focus on the 2D case only for simplicity and see how both QMC and MLQMC perform in practice when applied to equation (52). In figure 6 we study the adaptivity and cost of (ML)QMC as the root mean square error tolerance ε is decreased for the same FEM hierarchy, but for two different Haar level hierarchies. The top plots in the figure correspond to the choice of Haar meshes with mesh size comparable to the FEM mesh size ($|\square_{\mathcal{L}_\ell}|^{1/2} = 2^{-\ell}$). The results in the bottom plots are instead obtained by fixing the Haar level to $\mathcal{L}_\ell = 6$ for all ℓ . In both cases we fix the number of randomizations to be $M = 32$.

In the plots on the left hand side in figure 6 we see how MLQMC automatically selects the number of samples according to the greedy strategy highlighted in the supplementary material A and in [24] so as to satisfy the given error tolerance. As in the MLMC case, more samples are taken on coarse levels and only a few on the fine levels. The second Haar level strategy (figure 6, plot on the bottom right) uses higher Haar levels on the coarse MLQMC levels, which corresponds to a later decay to a $O(N^{-1/2})$ rate (cf. figure 5). Therefore this strategy requires lower sample sizes (compare with the top left plot).

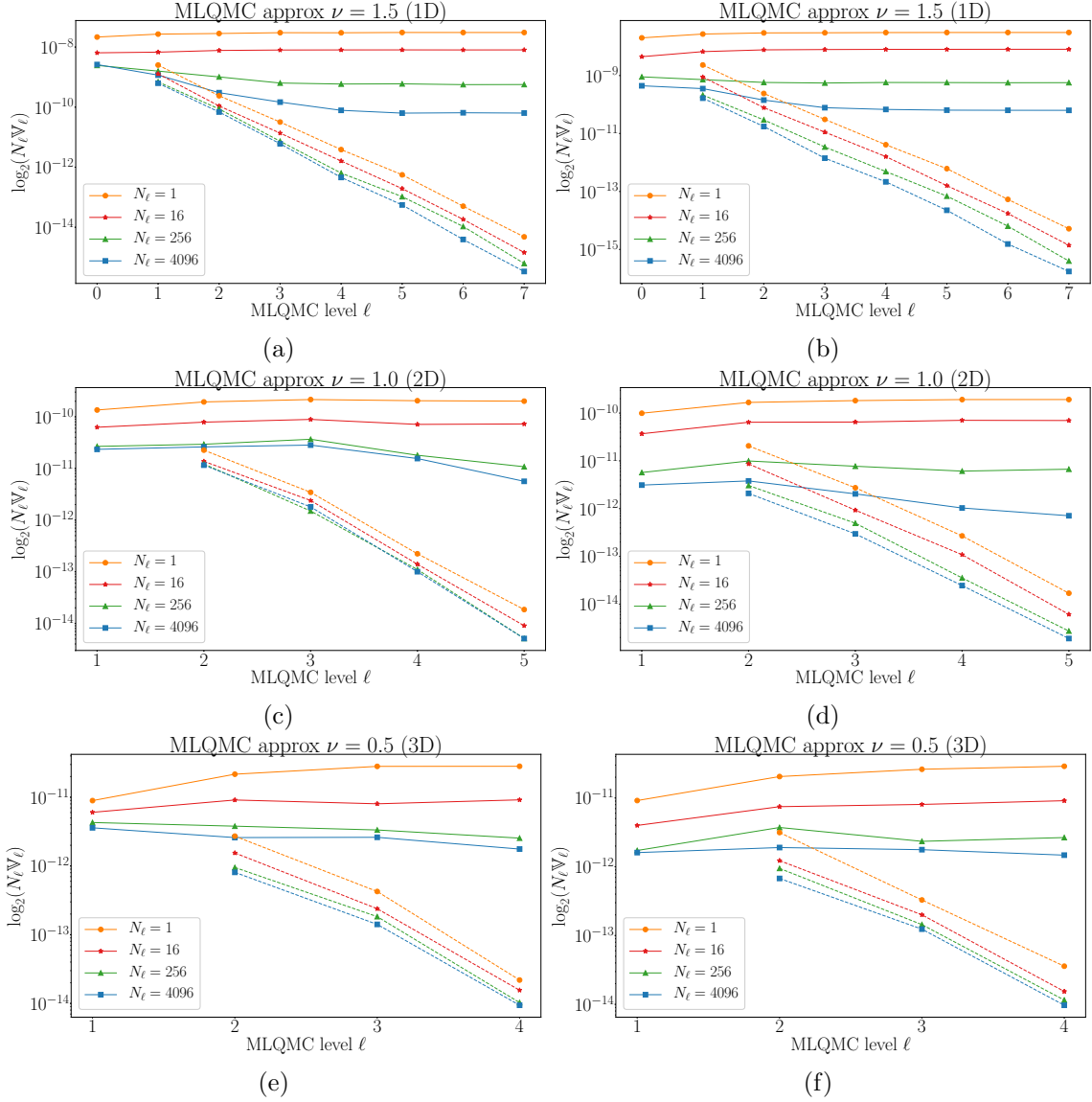


Figure 5: Convergence behaviour of (ML)QMC with respect to the number of samples N_ℓ in 1D (a)-(b) and 2D (c)-(d) ($M = 128$), and in 3D (e)-(f) ($M = 64$). Plots (a),(c),(e) (on the left) are obtained by choosing Haar mesh sizes comparable to the FEM mesh sizes: $|\square_{\mathcal{L}_\ell}| = 2^{-(\ell+1)}$ in 1D (a), and $|\square_{\mathcal{L}_\ell}|^{1/d} = 2^{-\ell}$ in 2D (c) and 3D (d). Plots (b),(d),(f) (on the right) are obtained by choosing Haar meshes which are finer than the corresponding FEM meshes: $|\square_{\mathcal{L}_\ell}| = 2^{-(\ell+2)}$ in 1D (b), $|\square_{\mathcal{L}_\ell}|^{1/2} = 2^{-(\ell+2)}$ in 2D (d) and $|\square_{\mathcal{L}_\ell}|^{1/3} = 2^{-(\ell+1)}$ in 3D (f). The (approximately) horizontal and oblique lines correspond to QMC and MLQMC respectively. Different colours indicate different sample sizes. On the y-axis we monitor (the logarithm of) the product between N_ℓ and the (ML)QMC estimator variance on level ℓ . This product is $O(1)$ when the convergence rate is MC-like and therefore the coloured lines would overlap if a $O(N^{-1/2})$ MC rate is observed. In the figure we observe a pre-asymptotic QMC-like convergence rate that then tails off to a standard MC rate (the lines initially do not overlap, but they get closer and closer as N_ℓ is increased). This phenomenon always occurs (cf. theorem B.1), but it happens later when the Haar level is increased (figures on the right).

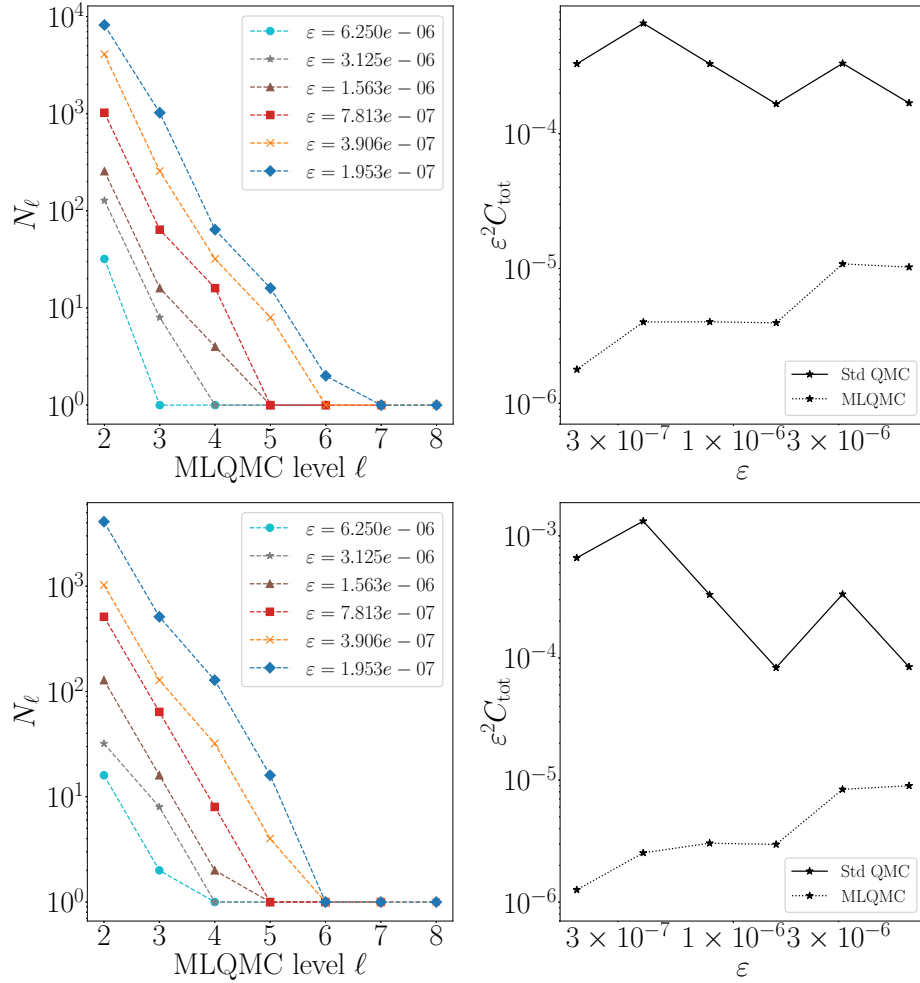


Figure 6: *MLQMC convergence for the solution of (52). We take $M = 32$ and consider two Haar level hierarchies: $\mathcal{L}_\ell = 2 + \ell$ (top plots) and $\mathcal{L}_\ell = 6$ for all ℓ (bottom plots). In the plots on the left we show how the MLQMC algorithm automatically selects the optimal number of samples N_ℓ on each level to achieve a given tolerance ε . Note that we have dropped the first mesh of the hierarchy as it is too coarse and it would not bring any significant advantage to the performance of MLQMC (same reasoning as for MLMC, see [25]). We observe that on the finest levels only one sample is used, making MLQMC equivalent to plain MLMC on these levels. In the plot on the right we compare the efficiency of MLQMC with QMC for different tolerances. MLQMC appears to have a better-than- $O(\varepsilon^{-2})$ total cost complexity and significantly outperforms QMC.*

In the plots on the right hand side we show the overall cost of QMC and MLQMC as the root mean square error tolerance ε is reduced. More specifically, we plot the quantity $\varepsilon^2 C_{\text{tot}}$, where C_{tot} is the total cost. The reason is that the total cost complexity of MLMC for this problem (MLMC parameters: $\beta = 2\alpha = 4$, $\gamma = 2$, cf. supplementary material A) is $O(\varepsilon^{-2})$, giving the $\varepsilon^2 C_{\text{tot}}$ factor to be $O(1)$ for all ε . The fact that the MLQMC cost line is not horizontal, but decreases as ε is reduced shows that the total complexity

of MLQMC is better than ε^{-2} , i.e. that our MLQMC algorithm has a better-than-MLMC complexity. This improved complexity stems from the fact that we are observing a QMC-like convergence rate with respect to N_ℓ .

As ε is decreased, we expect the cost complexity to decay to an ε^{-2} rate: for extremely fine tolerances very large sample sizes are required yielding the asymptotic $O(N^{-1/2})$ standard MC rate and harming the overall cost complexity. However, even in this case, the overall MLQMC cost benefits from the pre-asymptotic regime and MLQMC still outperforms MLMC (see figure 7). Similarly, QMC initially benefits from a faster convergence rate with respect to N . As the tolerance is decreased, the QMC rate decays to a standard MC rate and the total cost of QMC starts increasing faster than $O(\varepsilon^{-2})$.

Comparing the costs between the top and bottom of figure 6, it appears that increasing the Haar level on the coarse MLQMC levels improves the total MLQMC cost while, in the QMC case, decreasing the Haar level harms convergence. This suggests that the Haar level choice has a considerable impact on the overall MLQMC and QMC performance. We investigate this in figure 7, where we show the total cost of (ML)QMC for different Haar level hierarchies and we compare it with the cost of standard MLMC. The x -axis and the black lines in both plots are the same. We present the costs of two versions of MLMC: the black dash-dotted line corresponds to standard MLMC, while the black dashed line corresponds to a MLMC algorithm in which the number of samples are restricted to be in powers of 2 (this restriction also applies to the MLQMC algorithm we use [24]). MLQMC outperforms MLMC by a factor of approximately 8, depending on the Haar level choice.

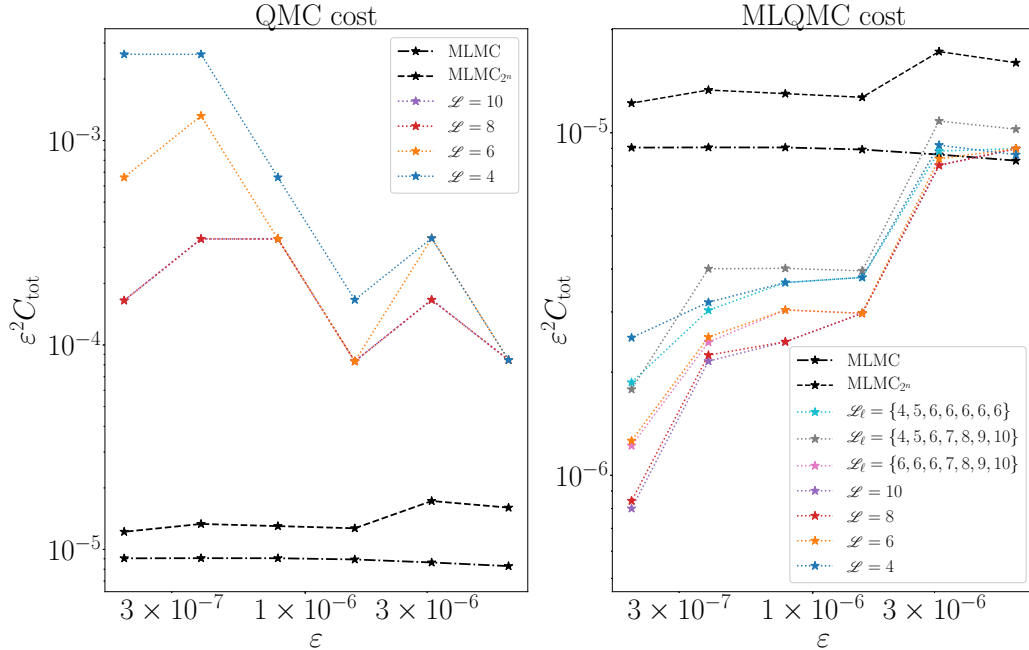


Figure 7: *MLMC*, *QMC* and *MLQMC* total computational cost needed for the solution of (52) with the same FEM mesh hierarchy as in figure 6. In the (ML)QMC case, we take $M = 32$ and consider different Haar level hierarchies which correspond to different computational costs. The x -axis and the MLMC lines are the same in both plots. MLQMC outperforms MLMC which in turn outperforms QMC.

Recall the convergence results with respect to the number of samples shown in figure 5: even if the convergence rate decreases as N_ℓ increases, it is clear from figure 6 (left) that this only happens on the coarse levels where more samples are needed. Since for problem (52) and the FEM discretization chosen we are in the “good” case of the MLMC theorem (i.e. $\beta > \gamma$, cf. theorem A.1 in the supplementary material), the multilevel cost is dominated by the sample cost on the coarse levels. We therefore expect to obtain computational gains by increasing the Haar level on the coarse MLQMC levels. At the same time, we do not expect to lose in computational efficiency if we decrease the Haar level on the fine levels as these are not dominating the total cost. Note that in the QMC case there is only one level and the only possible strategy is to keep the Haar level as high as required.

Remark 6.3. The results shown in figures 6 and 7 do not account for differences in the cost per sample due to variations in the number of supermesh cells. If the cost of solving the PDE with random coefficients of interest (e.g. equation (52)) dominates over the cost of sampling white noise realizations, these results are still valid as is. Otherwise, extra care must be taken when using Haar meshes which are much finer than the corresponding FEM meshes as this results in a large number of supermesh cells. In the figures this would apply to Haar levels greater than $\mathcal{L}_\ell = \{4, \dots, 10\}$ (gray line in the plot on the right) and there is clearly a trade-off: larger \mathcal{L} means faster decay with respect to N , but larger costs per sample as well.

By looking at figure 7 it is clear that our expectations are met. In the QMC case (plot on the left) we see that a small Haar level results in significant cost increase for small tolerances, while for large Haar levels we retain good convergence with respect to N and a cost complexity which looks just slightly worse than $O(\varepsilon^{-2})$. For the tolerances considered, there seems to be little advantage in increasing the Haar level beyond the $\mathcal{L} = 8$ threshold. For this specific problem, the optimal strategy would be to increase the Haar level as the mesh is refined and set $\mathcal{L}_\ell = \{4, 5, 6, 6, 8, 8\}$ so that the Haar level is increased only when needed. Generally speaking, we believe that it is never advantageous to use Haar meshes much finer than the FEM meshes (cf. remark 6.3).

In the MLQMC case (plot on the right in figure 7), we note that increasing the Haar level on the coarse levels indeed brings computational advantages (e.g. compare the gray and pink lines) and decreasing it on the fine levels does not seem to affect the total cost (e.g. compare the pink with the orange line), as predicted. The optimal strategy therefore consists of increasing the Haar level on the coarse levels and either keeping it constant across the MLQMC hierarchy or possibly even decreasing it (there is little computational advantage in decreasing it if the FEM meshes on the fine levels are already much finer than the Haar mesh). For the MLQMC hierarchy, a good choice seems to fix $\mathcal{L}_\ell = 6$ for all ℓ since a larger Haar level would significantly increase the number of supermesh cells (cf. remark 6.3).

Overall, our MLQMC strategy outperforms MLMC, which in turn outperforms QMC. Standard MC is always worse than QMC, by up to two orders of magnitude for small ε (not shown).

Remark 6.4. The optimal Haar strategy is likely to change if the problem to be solved belongs to the other two cases of the MLMC theorem (theorem A.1 in the supplementary material), i.e. $\beta = \gamma$ or $\beta < \gamma$. In the first case ($\beta = \gamma$), the total multilevel cost is

simultaneously dominated by all levels in the multilevel hierarchy and we expect in this case that the optimal strategy is to use a Haar mesh hierarchy of mesh sizes comparable to the FEM mesh sizes (e.g. as for the gray line in the right plot of figure 7). In the latter case ($\beta < \gamma$), the total multilevel cost is dominated by the fine levels. In this case it might be advantageous to keep the Haar level low on the coarse levels and to increase it on the fine levels.

Remark 6.5. If we are in the $\beta > \gamma$ case, then the Haar level is capped on the fine levels. Therefore, as previously mentioned in remarks 4.3 and 5.1, the overall white noise sampling complexity is asymptotically linear with respect to the number of cells of the FEM mesh considered even in the case in which we are using standard Haar wavelets (cf. remark 3.1). In the other cases of the MLMC theorem (theorem A.1 in the supplementary material), it might be detrimental to cap the Haar level and non-standard Haar wavelets are to be preferred in case we cannot afford the additional logarithmic term in the complexity estimate.

7 Conclusions

We presented a novel algorithm to efficiently compute the action of white noise and sample Matérn fields within a QMC and MLQMC framework. This algorithm retains the computational efficiency of the MLMC case [13] and still enforces the required multilevel coupling in a non-nested mesh hierarchy. The numerical results show that our technique works well in practice, that the convergence orders observed agree with the theory and that MLQMC outperforms MLMC and has a better cost complexity in the pre-asymptotic regime. We remark that the sampling technique presented extends naturally to any application in which spatial white noise realizations are needed within a finite element framework provided that the solution is smooth enough. An open problem is the derivation of a closed-form expression for the optimal number of samples on each MLQMC level and for the optimal Haar level hierarchy, but we leave this to future research. It would also be interesting to extend the algorithms presented to general higher degree wavelets and domains (cf. remarks 5.4 and 5.5). The first enhancement (generic wavelets) could possibly improve the convergence rate with respect to the number of samples, while the second (general domains) would reduce the supermeshing complexity and consequently the white noise sample cost.

Acknowledgments

The authors would like to acknowledge useful discussions with Marie Rognes, Abdul-Lateef Haji-Ali, Alberto Paganini and Casper Beentjes. The authors would also like to express their thanks to James R. Maddison for his assistance with the implementation of an interface between libsupermesh and FEniCS.

References

- [1] M. Bachmayr et al. *Unified Analysis of Periodization-Based Sampling Methods for Matérn Covariances*. 2019.

- [2] S. Balay et al. *PETSc users manual revision 3.8*. Tech. rep. Argonne National Laboratory (ANL), 2017.
- [3] C. H. L. Beentjes and R. E. Baker. “Quasi-Monte Carlo methods applied to tau-leaping in stochastic biological systems”. In: *Bulletin of Mathematical Biology* (2018), pp. 1–29.
- [4] G. Beylkin et al. “Wavelets in numerical analysis”. In: *Wavelets and their Applications*. Vol. 181. Jones & Bartlett Boston, 1992, pp. 1–28.
- [5] D. Bolin and K. Kirchner. *The SPDE approach for Gaussian random fields with general smoothness*. 2017.
- [6] D. Bolin et al. “Numerical solution of fractional elliptic stochastic PDEs with spatial white noise”. In: *IMA Journal of Numerical Analysis* dry091 (2018), pp. 1–23.
- [7] S. Brenner and R. L. Scott. *The Mathematical Theory of Finite Element Methods*. Vol. 15. Springer Science and Business Media, 1994.
- [8] R. E. Caflish et al. “Valuation of mortgage-backed securities using Brownian bridges to reduce effective dimension”. In: *Journal of Computational Finance* 1 (1997), pp. 27–46.
- [9] K. A. Cliffe et al. “Multilevel Monte Carlo methods and applications to elliptic PDEs with random coefficients”. In: *Computing and Visualization in Science* 14.1 (2011), pp. 3–15.
- [10] S. G. Cox and K. Kirchner. *Regularity and convergence analysis in Sobolev and Hölder spaces for generalized Whittle-Matérn fields*. 2019.
- [11] M. Croci. “Multilevel Monte Carlo methods for uncertainty quantification in brain simulations”. PhD thesis. University of Oxford, 2019.
- [12] M. Croci and P. E. Farrell. *Complexity bounds on supermesh construction for quasi-uniform meshes*. 2019. URL: <https://arxiv.org/abs/1911.11589>.
- [13] M. Croci et al. “Efficient white noise sampling and coupling for multilevel Monte Carlo with non-nested meshes”. In: *SIAM/ASA Journal on Uncertainty Quantification* 6.4 (2018), pp. 1630–1655.
- [14] I. Daubechies. “Orthonormal bases of compactly supported wavelets”. In: *Communications on Pure and Applied Mathematics* 41.7 (1988), pp. 909–996.
- [15] J. Dick et al. “High-dimensional integration: the quasi-Monte Carlo way”. In: *Acta Numerica* (2013), pp. 133–288.
- [16] C. R. Dietrich and G. N. Newsam. “Fast and exact simulation of stationary Gaussian processes through circulant embedding of the covariance matrix”. In: *SIAM Journal on Scientific Computing* 18.4 (1997), pp. 1088–1107.
- [17] J. Dölz et al. “Covariance regularity and \mathcal{H} -matrix approximation for rough random fields”. In: *Numerische Mathematik* 135.4 (2017), pp. 1045–1071.
- [18] R. D. Falgout and U. M. Yang. “*Hypre*: A library of high performance preconditioners”. In: *International Conference on Computational Science*. Springer, 2002, pp. 632–641.

- [19] P. E. Farrell. “Galerkin projection of discrete fields via supermesh construction”. PhD thesis. Imperial College London, 2009.
- [20] P. E. Farrell and J. R. Maddison. “Conservative interpolation between volume meshes by local Galerkin projection”. In: *Computer Methods in Applied Mechanics and Engineering* 200 (2011), pp. 89–100.
- [21] P. E. Farrell et al. “Conservative interpolation between unstructured meshes via supermesh construction”. In: *Computer Methods in Applied Mechanics and Engineering* 198 (2009), pp. 2632–2642.
- [22] M. Feischl et al. “Fast random field generation with H-matrices”. In: *Numerische Mathematik* 140 (2018), pp. 639–676.
- [23] D. Gilbarg and N. S. Trudinger. *Elliptic Partial Differential Equations of Second Order*. Springer-Verlag, 2015.
- [24] M. B. Giles and B. J. Waterhouse. “Multilevel quasi-Monte Carlo path simulation”. In: *Advanced Financial Modelling (Radon Series on Computational and Applied Mathematics)*. 8. De Gruyter, 2009, pp. 165–181.
- [25] M. B. Giles. “Multilevel Monte Carlo methods”. In: *Acta Numerica* 24 (2015), pp. 259–328.
- [26] M. B. Giles. “Multilevel Monte Carlo path simulation”. In: *Operations Research* 56.3 (2008), pp. 607–617.
- [27] P. Glasserman. *Monte Carlo Methods in Financial Engineering*. Springer Science & Business Media, 2013.
- [28] I. G. Graham et al. “Analysis of circulant embedding methods for sampling stationary random fields”. In: *SIAM Journal on Numerical Analysis* 56.3 (2018), pp. 1871–1895.
- [29] I. G. Graham et al. “Quasi-Monte Carlo finite element methods for elliptic PDEs with log-normal random coefficients”. In: *Numerische Mathematik* 131.2 (2013), pp. 329–368.
- [30] W. Hackbusch. *Elliptic Differential Equations: Theory and Numerical Treatment*. Springer-Verlag, 1992.
- [31] W. Hackbusch. *Hierarchical Matrices: Algorithms and Analysis*. Springer, 2015, p. 511.
- [32] A.-L. Haji-Ali et al. “Optimization of mesh hierarchies in multilevel Monte Carlo samplers”. In: *Stochastics and Partial Differential Equations Analysis and Computations* 4.1 (2016), pp. 76–112.
- [33] S. Heinrich. “Multilevel Monte Carlo Methods”. In: *Large-Scale Scientific Computing*. Berlin, Heidelberg: Springer Berlin Heidelberg, 2001, pp. 58–67.
- [34] L. Herrmann and C. Schwab. “Multilevel quasi-Monte Carlo integration with product weights for elliptic PDEs with lognormal coefficients”. In: *ESAIM: Mathematical Modelling and Numerical Analysis* 53.5 (2019), pp. 1507–1552.
- [35] T. Hida et al. *White Noise: an Infinite Dimensional Calculus*. 1st ed. Springer Science & Business Media, 1993.

- [36] H. Inaba and B. D. Tapley. “Generalized random processes: a theory and the white Gaussian process”. In: *SIAM Journal on Control* 13.3 (1975), pp. 719–735.
- [37] S. Joe and F. Y. Kuo. “Constructing Sobol sequences with better two-dimensional projections”. In: *SIAM Journal on Scientific Computing* 30.5 (2008), pp. 2635–2654.
- [38] B. N. Khoromskij et al. “Application of hierarchical matrices for computing the Karhunen-Loève expansion”. In: *Computing* 84.1-2 (2009), pp. 49–67.
- [39] U Khristenko et al. *Analysis of boundary effects on PDE-based sampling of Whittle-Matérn random fields*. 2018.
- [40] I. Kiyosi. “Stationary random distributions”. In: *Memoirs of the College of Science, University of Kyoto. Series A: Mathematics* 28.3 (1954), pp. 209–223.
- [41] F. Y. Kuo et al. “Multi-level quasi-Monte Carlo finite element methods for a class of elliptic PDEs with random coefficients”. In: *Foundations of Computational Mathematics* 15.2 (2015), pp. 411–449.
- [42] F. Y. Kuo et al. “Multilevel quasi-Monte Carlo methods for lognormal diffusion problems”. In: *Mathematics of Computation* 86.308 (2017), pp. 2827–2860.
- [43] F. Y. Kuo and D. Nuyens. *A practical guide to quasi-Monte Carlo methods*. Tech. rep. KU Leuven, 2016, pp. 1–50.
- [44] P. L’Ecuyer and C. Lemieux. “Variance reduction via lattice rules”. In: *Management Science* 46.9 (2000), pp. 1214–1235.
- [45] C. Lemieux. *Monte Carlo and Quasi-Monte Carlo Sampling*. 1st ed. Springer Series in Statistics. Springer-Verlag New York, 2009.
- [46] F. Lindgren et al. “An explicit link between Gaussian fields and Gaussian Markov random fields: the stochastic partial differential equation approach”. In: *Journal of the Royal Statistical Society: Series B (Statistical Methodology)* 73.4 (2009), pp. 423–498.
- [47] A. Logg et al. *Automated Solution of Differential Equations by the Finite Element Method: the FEniCS Book*. Vol. 84. Springer Science & Business Media, 2012.
- [48] J. R. Maddison et al. *Parallel supermeshing for multimesh modelling*. Tech. rep. Archer, eCSE03-08, 2013. URL: <https://arxiv.org/abs/1911.11589>.
- [49] W. J. Morokoff and R. E. Caflisch. “Quasi-Monte Carlo integration”. In: *Journal of Computational Physics* 122.2 (1995), pp. 218–230.
- [50] S. Osborn et al. *A multilevel, hierarchical sampling technique for spatially correlated random fields*. 2017.
- [51] A. B. Owen. “Randomly permuted (t, m, s) -nets and (t, s) -sequences.” In: *Monte Carlo and Quasi-Monte Carlo Methods in Scientific Computing*. Springer, New York, NY, 1995, pp. 299–317.
- [52] A. B. Owen. “Scrambled net variance for integrals of smooth functions”. In: *Annals of Statistics* 25.4 (1997), pp. 1541–1562.
- [53] A. B. Owen. “Scrambling Sobol’ and Niederreiter-Xing points”. In: *Journal of Complexity* 14 (1998), pp. 466–489.

- [54] A. B. Owen. “Variance and discrepancy with alternative scramblings”. In: *ACM Transactions on Modeling and Computer Simulation* 13.4 (2003), pp. 363–378.
- [55] P. Whittle. “On stationary processes in the plane”. In: *Biometrika* 41.3-4 (1954), pp. 434–449.
- [56] R. Potsepaev and C. L. Farmer. “Application of stochastic partial differential equations to reservoir property modelling”. In: *ECMOR XII-12th European Conference on the Mathematics of Oil Recovery*. Vol. 2. September. 2014.
- [57] I. M. Sobol’ et al. “Construction and comparison of high-dimensional Sobol’ generators”. In: *Wilmott* Nov. 2011.56 (2011), pp. 64–79.
- [58] T. J. Sullivan. *Introduction to Uncertainty Quantification*. Vol. 63. Springer, 2015.
- [59] A. L. Teckentrup et al. “Further analysis of multilevel Monte Carlo methods for elliptic PDEs with random coefficients”. In: *Numerische Mathematik* 125.3 (2013), pp. 569–600.
- [60] A. T. A. Wood and G. Chan. “Simulation of stationary Gaussian processes in $[0, 1]^d$ ”. In: *Journal of Computational and Graphical Statistics* 3.4 (1994), pp. 409–432.

Supplementary material

Multilevel quasi Monte Carlo methods for elliptic PDEs with random field coefficients via fast white noise sampling

M. Croci, M. B. Giles, P. E. Farrell

A Multilevel Monte Carlo methods

A.1 MLMC convergence theory

We briefly summarize the MLMC convergence theory since it is useful to understand some of the considerations drawn in section 6.

The MSE of the MLMC estimator is given by,

$$MSE = \hat{V} + E[\hat{P} - P]^2, \quad (53)$$

where \hat{P} is the MLMC estimator of variance \hat{V} . To ensure that $MSE \leq \varepsilon^2$, we enforce the bounds,

$$\hat{V} \leq (1 - \theta)\varepsilon^2, \quad E[\hat{P} - P]^2 \leq \theta\varepsilon^2, \quad (54)$$

where $\theta \in (0, 1)$ is a weight, introduced by Haji-Ali et al. in [32]. Let C_ℓ, V_ℓ be the cost and variance of one sample $(P_\ell - P_{\ell-1})(\omega)$ respectively. Then the total MLMC cost and variance are

$$C_{tot} = \sum_{\ell=1}^L N_\ell C_\ell, \quad \hat{V} = \sum_{\ell=1}^L N_\ell^{-1} V_\ell. \quad (55)$$

We can minimise the estimator variance for fixed total cost. For further details we refer to [25]. This gives that, for a fixed MSE tolerance ε^2 , the optimal number of samples for each level and related total cost are,

$$N_\ell = \left(\varepsilon^{-2} \sum_{\ell=1}^L \sqrt{V_\ell C_\ell} \right) \sqrt{V_\ell / C_\ell}, \quad C_{tot} = \varepsilon^{-2} \left(\sum_{\ell=1}^L \sqrt{V_\ell C_\ell} \right)^2. \quad (56)$$

We can now compare the cost complexity of standard and multilevel Monte Carlo for the estimation of $\mathbb{E}[P_L]$. Usually, $\mathbb{V}[P_L] = O(V_1)$, then the total cost complexity of standard MC is $O(\varepsilon^{-2} V_1 C_L)$. According to how the product $V_\ell C_\ell$ varies with level, we can have three different scenarios for MLMC:

1. The product $V_\ell C_\ell$ increases with level ($\gamma > \beta$ in theorem A.1, to follow). Then, to leading order, the total MLMC cost is $O(\varepsilon^{-2} V_L C_L)$, for an improvement in computational cost over standard Monte Carlo by a V_1/V_L factor. In this case the total cost is dominated by the fine levels.
2. The product is asymptotically constant with the level. Then, we have a MLMC total cost of order $O(\varepsilon^{-2} L^2 V_L C_L) = O(\varepsilon^{-2} L^2 V_1 C_1)$ ($\gamma = \beta$ in theorem A.1, to follow). This gives a cost improvement of $V_1/(L^2 V_L) \approx C_L/(L^2 C_1)$ with respect to standard MC. The MLMC cost here is equally dominated by all the levels in the hierarchy.

3. The product decreases with the level ($\gamma < \beta$ in theorem A.1, to follow). Then, $C_{tot} \approx O(\varepsilon^{-2} V_L C_1)$, for an improvement of C_L/C_1 . For example this could be the ratio between a fine mesh PDE solution cost and a coarse mesh PDE solution cost, which is generally quite significant. In this case, the MLMC cost is dominated by the coarser levels.

The convergence of MLMC is ensured by the following theorem.

Theorem A.1 ([25], theorem 1). *Let $P \in L^2(\Omega, \mathbb{R})$ and let P_ℓ be its level ℓ approximation. Let Y_ℓ be the MC estimator of $\mathbb{E}[P_\ell - P_{\ell-1}]$ on level ℓ such that*

$$\mathbb{E}[Y_\ell] = \mathbb{E}[P_\ell - P_{\ell-1}], \quad (57)$$

with $P_0 = 0$, and let C_ℓ and V_ℓ the expected cost and variance of each of the N_ℓ Monte Carlo samples needed to compute Y_ℓ . If the estimators Y_ℓ are independent and there exist positive constants $\alpha, \beta, \gamma, c_1, c_2, c_3$, such that $\alpha \geq \frac{1}{2} \min(\beta, \gamma)$ and

$$|\mathbb{E}[P_\ell - P]| \leq c_1 2^{-\alpha\ell}, \quad V_\ell \leq c_2 2^{-\beta\ell}, \quad C_\ell \leq c_3 2^{\gamma\ell}, \quad (58)$$

then there exist a positive constant c_4 such that, for all $\varepsilon < e^{-1}$, there is a level number L and number of samples N_ℓ , such that the MLMC estimator

$$\hat{P} = \sum_{\ell=1}^L Y_\ell, \quad (59)$$

has MSE with bound,

$$MSE = \mathbb{E}[(\hat{P} - \mathbb{E}[P])^2] \leq \varepsilon^2, \quad (60)$$

with a total computational complexity with bound,

$$\mathbb{E}[C_{tot}] \leq \begin{cases} c_4 \varepsilon^{-2}, & \beta > \gamma, \\ c_4 \varepsilon^{-2} (\log \varepsilon)^2, & \beta = \gamma, \\ c_4 \varepsilon^{-2 - (\gamma - \beta)/\alpha}, & \beta < \gamma. \end{cases} \quad (61)$$

A.2 MLQMC algorithm

Let C_ℓ be the cost of evaluating Y_ℓ and let $V_\ell = \mathbb{V}[I_{N_\ell}^{m,\ell}]$, where $I_{N_\ell}^{m,\ell}$ is given in (9). The MLQMC algorithm we adopt, taken from [24], is the following.

MLQMC algorithm (taken from [24])

1. Set the required tolerance ε , $\theta \in (0, 1)$, the minimum and maximum level L_{\min} and L_{\max} and the initial number of levels to be $L = 1$.
2. Get an initial estimate of V_L with $N_L = 1$ and $M = 32$ randomizations.
3. While $\sum_{\ell=1}^L V_\ell > (1 - \theta)\varepsilon^2$, double N_ℓ on the level with largest $V_\ell/(C_\ell N_\ell)$.

4. If $L < L_{\min}$ or the bias estimate is greater than $\sqrt{\theta}\varepsilon$, set $L = L + 1$. If $L \leq L_{\max}$ go to 2, otherwise report convergence failure.

Remark A.1 (Adapted from [24]). The term $\sum_{\ell=1}^L V_\ell$ is the total estimator variance and the variable θ is a weight with the same meaning as in the MLMC case. The choice of N_ℓ on each level is heuristic: doubling the number of samples will eliminate (independently on whether we are in an MC or QMC-like convergence rate regime) most of the estimated variance V_ℓ on level ℓ at a cost $N_\ell C_\ell$ and we therefore double the number of samples on the level that offers the largest variance reduction per unit cost.

B A partial QMC convergence result

The white noise sampling strategy we presented is hybrid in the sense that both randomized low-discrepancy and pseudo-random sequences are used. It is then unclear what the order of convergence with respect to the number of samples should be. The hope is, of course, to achieve something better than the standard MC rate of convergence. Proving convergence results with respect to the number of samples for QMC (and MLQMC) in a PDE setting is non-trivial and results have so far been established only for a limited class of low-discrepancy sequences [34, 42].

Although deriving a convergence estimate is outside of the scope of this work, in what follows we try to build up intuition about what is likely to be happening in practice. As an example problem, consider the following elliptic PDE with log-normal diffusion coefficient (already in weak form): find $p(\cdot, \omega) \in H_0^1(G)$ such that for all $v \in H_0^1(G)$,

$$a(p, v) = (D^*(\mathbf{x}, \omega) \nabla p, \nabla v) = (f, v), \quad \text{a.s.}, \quad D^*(\mathbf{x}, \omega) = e^{u(\mathbf{x}, \omega)}, \quad (62)$$

where for a given sampling domain $D \subset \subset \mathbb{R}^d$ we have that $G \subset \subset D$ is a domain of class $C^{1, \epsilon}$ for any $\epsilon > 0$, $f \in L^\infty(G)$ (these hypotheses imply $p \in W^{1, \infty}(G)$ a.s., see theorem 8.34 in [23]) and $u(\mathbf{x}, \omega)$ is a Matérn field satisfying equation (15) over D . In addition, assume that we are interested in computing the expectation of a possibly nonlinear output functional of p , namely $\mathcal{P}(p)$. We will now establish the following result:

Theorem B.1. *Let $p \in W^{1, \infty}(G)$ a.s. be the solution of (62) where $u \in H^s(G)$ a.s. has been sampled using the hybrid QMC technique presented in this paper. Let $u_{\mathcal{L}}$ be the solution of (15) obtained by using the same $\dot{W}_{\mathcal{L}}$ sample as for u and by setting $\dot{W}_R = 0$, and let $p_{\mathcal{L}}(\cdot, \omega) \in H_0^1(G)$ satisfy, for all $v \in H_0^1(G)$,*

$$a_{\mathcal{L}}(p_{\mathcal{L}}, v) = (D_{\mathcal{L}}^*(\mathbf{x}, \omega) \nabla p_{\mathcal{L}}, \nabla v) = (f, v), \quad \text{a.s.}, \quad D_{\mathcal{L}}^*(\mathbf{x}, \omega) = e^{u_{\mathcal{L}}(\mathbf{x}, \omega)}. \quad (63)$$

Let $\mu = \min(s, 1)$ and let \mathcal{L} be the Haar level used to sample u . Assume that the functional \mathcal{P} is continuously Fréchet differentiable and let $\hat{P}, \hat{P}_{\mathcal{L}}$ and $\widehat{P - P_{\mathcal{L}}}$ be the QMC estimators for $\mathbb{E}[P]$, $\mathbb{E}[P_{\mathcal{L}}]$ and $\mathbb{E}[P - P_{\mathcal{L}}]$ respectively, obtained by using N QMC points. Here, $P = \mathcal{P}(p)$ and $P_{\mathcal{L}} = \mathcal{P}(p_{\mathcal{L}})$. If there exist two constants $c > 0$ and $q \geq 1$ such that the QMC estimators asymptotically satisfy as $N \rightarrow \infty$,

$$\mathbb{V}[\hat{P}] \leq c \frac{\mathbb{V}[P]}{N}, \quad \mathbb{V}[\hat{P}_{\mathcal{L}}] \leq c \frac{\mathbb{V}[P_{\mathcal{L}}]}{N^q}, \quad \mathbb{V}[\widehat{P - P_{\mathcal{L}}}] \leq c \frac{\mathbb{V}[P - P_{\mathcal{L}}]}{N}, \quad (64)$$

i.e. the QMC estimators are never asymptotically worse than standard Monte Carlo, then the statistical error $\mathbb{V}[\hat{P}]$ also asymptotically satisfies as $N, \mathcal{L} \rightarrow \infty$,

$$\mathbb{V}[\hat{P}] \leq \frac{c}{N^q} + \frac{\bar{c}}{N} 2^{-\mu \mathcal{L}}, \quad (65)$$

where $\bar{c} > 0$ is independent from \mathcal{L} and N .

Remark B.1. Condition (64) is satisfied by most randomized low-discrepancy point sets, e.g. randomized digital nets and sequences and randomly shifted lattice rules [44, 51, 52, 53].

Proof. We start with essentially the same duality argument that yields lemma 3.2 in [59]. Let $v, \bar{v} \in H^1(G)$ and let $D_v \mathcal{P}(\bar{v})$ be the Gateaux derivative of \mathcal{P} at \bar{v} , namely

$$D_v \mathcal{P}(\bar{v}) := \lim_{\epsilon \rightarrow 0} \frac{\mathcal{P}(\bar{v} + \epsilon v) - \mathcal{P}(\bar{v})}{\epsilon}. \quad (66)$$

Define the average derivative of \mathcal{P} on the path from p to $p_{\mathcal{L}}$,

$$\overline{D_v \mathcal{P}}(p, p_{\mathcal{L}}) = \int_0^1 D_v \mathcal{P}(p + \theta(p_{\mathcal{L}} - p)) \, d\theta, \quad (67)$$

and introduce the dual problem: find $z(\cdot, \omega) \in H_0^1(G)$ s.t.

$$a(v, z) = \overline{D_v \mathcal{P}}(p, p_{\mathcal{L}}), \quad \forall v \in H_0^1(G). \quad (68)$$

The fundamental theorem of calculus for Fréchet derivatives then yields,

$$P - P_{\mathcal{L}} = \int_0^1 D_{p-p_{\mathcal{L}}} \mathcal{P}(p + \theta(p_{\mathcal{L}} - p)) \, d\theta = \overline{D_{p-p_{\mathcal{L}}} \mathcal{P}}(p, p_{\mathcal{L}}) = a(p - p_{\mathcal{L}}, z), \quad \text{a.s.} \quad (69)$$

Applying Hölder's inequality gives,

$$|P - P_{\mathcal{L}}| = |a(p - p_{\mathcal{L}}, z)| \leq \|D^*\|_{L^\infty(G)} |z|_{H^1(G)} |p - p_{\mathcal{L}}|_{H^1(G)} \quad \text{a.s.} \quad (70)$$

We now need a bound for $|p - p_{\mathcal{L}}|_{H^1(G)}$. Note that, a.s. for all $v \in H_0^1(G)$,

$$0 = a(p, v) - a_{\mathcal{L}}(p_{\mathcal{L}}, v) = a(p - p_{\mathcal{L}}, v) + a(p_{\mathcal{L}}, v) - a_{\mathcal{L}}(p_{\mathcal{L}}, v). \quad (71)$$

Setting $v = p - p_{\mathcal{L}}$ gives

$$0 \leq a(p - p_{\mathcal{L}}, p - p_{\mathcal{L}}) = a_{\mathcal{L}}(p_{\mathcal{L}}, v) - a(p_{\mathcal{L}}, v) = ((D_{\mathcal{L}}^* - D^*) \nabla p_{\mathcal{L}}, \nabla(p - p_{\mathcal{L}})) \quad \text{a.s.} \quad (72)$$

Both quantities can be bounded as follows: let $D_{\min}^*(\omega) = \inf_{x \in D} |D^*(\cdot, \omega)|$,

$$0 \leq D_{\min}^* |p - p_{\mathcal{L}}|_{H_0^1(G)}^2 \leq a(p - p_{\mathcal{L}}, p - p_{\mathcal{L}}) \quad (73)$$

$$((D_{\mathcal{L}}^* - D^*) \nabla p_{\mathcal{L}}, \nabla(p - p_{\mathcal{L}})) \leq \|D^* - D_{\mathcal{L}}^*\|_{L^2(G)} \|\nabla p\|_{L^\infty(G)} |p - p_{\mathcal{L}}|_{H^1(G)}, \quad (74)$$

almost surely, hence yielding, after division by $|p - p_{\mathcal{L}}|_{H^1(G)}$,

$$|p - p_{\mathcal{L}}|_{H^1(G)} \leq \frac{\|D^*\|_{L^\infty(G)}^\alpha}{D_{\min}^*} \|\nabla p\|_{L^\infty(G)} \|u - u_{\mathcal{L}}\|_{L^2(G)}, \quad \text{a.s.}, \quad (75)$$

for some $\alpha \geq 1$. Here we used the fact that since $u_{\mathcal{L}}$ converges to u in $C^{2-d/2-\epsilon}(D)$ for any $\epsilon > 0$ [10] (and consequently in $C^{2-d/2-\epsilon}(G)$), there exists a Haar level \mathcal{L}_0 such that for all $\mathcal{L} > \mathcal{L}_0$ there exists a constant $\alpha \geq 1$ independent from \mathcal{L} such that $\|u_{\mathcal{L}}\|_{L^\infty(G)} \leq \alpha \|u\|_{L^\infty(G)}$, hence

$$\|D^* - D_{\mathcal{L}}^*\|_{L^2(G)} \leq e^{\max(\|u\|_{L^\infty(G)}, \|u_{\mathcal{L}}\|_{L^\infty(G)})} \|u - u_{\mathcal{L}}\|_{L^2(G)} \quad (76)$$

$$\leq \|D^*\|_{L^\infty(G)}^\alpha \|u - u_{\mathcal{L}}\|_{L^2(G)}, \quad \text{a.s.} \quad (77)$$

Putting (70) and (75) together yields,

$$|P - P_{\mathcal{L}}| \leq C(\omega) \|u - u_{\mathcal{L}}\|_{L^2(G)}, \quad \text{a.s.}, \quad (78)$$

where $C(\omega) \in L^p(\Omega, \mathbb{R})$ for all $p \in (0, \infty)$ and is given by

$$C(\omega) = \frac{\|D^*\|_{L^\infty(G)}^{\alpha+1}}{D_{\min}^*} \|\nabla p\|_{L^\infty(G)} |z|_{H^1(G)}. \quad (79)$$

We now note that

$$\begin{aligned} \mathbb{V}[\hat{P}] &= \mathbb{V}[\hat{P}_{\mathcal{L}} + \hat{P} - \hat{P}_{\mathcal{L}}] = \mathbb{V}[\hat{P}_{\mathcal{L}}] + \text{Cov}(\hat{P} + \hat{P}_{\mathcal{L}}, \hat{P} - \hat{P}_{\mathcal{L}}) \\ &\leq \mathbb{V}[\hat{P}_{\mathcal{L}}] + \mathbb{V}[\hat{P} + \hat{P}_{\mathcal{L}}]^{1/2} \mathbb{V}[(\widehat{P - P_{\mathcal{L}}})]^{1/2} \end{aligned} \quad (80)$$

$$\leq c \frac{\mathbb{V}[P_{\mathcal{L}}]}{N^q} + \frac{c\tilde{c}}{N} \mathbb{V}[P]^{1/2} \mathbb{V}[P - P_{\mathcal{L}}]^{1/2}. \quad (81)$$

where we used the Cauchy-Schwarz inequality, hypothesis (64) and the fact that since P converges to $P_{\mathcal{L}}$ as $\mathcal{L} \rightarrow \infty$ a.s. and in $L^p(\Omega, \mathbb{R})$ for $p \in (0, \infty)$, there exists a Haar level \mathcal{L}_0 s.t. for all $\mathcal{L} > \mathcal{L}_0$ there exists $c_1 > 0$ s.t. $\mathbb{V}[P_{\mathcal{L}}] \leq c_1 \mathbb{V}[P]$ and consequently another constant $\tilde{c} > 0$ s.t. $\mathbb{V}[P + P_{\mathcal{L}}]^{1/2} \leq \tilde{c} \mathbb{V}[P]^{1/2}$. Combining equation (78) with Cauchy-Schwarz and the embedding $L^4(G) \subset L^2(G)$ gives that

$$\mathbb{V}[P - P_{\mathcal{L}}]^{1/2} \leq |D|^{1/4} \mathbb{E}[C(\omega)^4]^{1/4} \mathbb{E}[\|u - u_{\mathcal{L}}\|_{L^4(G)}^4]^{1/4}. \quad (82)$$

Now, since $\dot{W}_{\mathcal{L}}$ is the projection of \dot{W} onto V_H , the same argument as in the proof for lemma 3.8 in [11] can be used to obtain the estimate

$$\mathbb{E}[\|u - u_{\mathcal{L}}\|_{L^4(G)}^4]^{1/4} \leq \bar{C}(s, D, d) |\square_H|^{\mu/d}, \quad (83)$$

for some constant \bar{C} . The argument follows by replacing V_h with the Haar mesh subspace V_H (of polynomial degree 0), h with the Haar mesh size $|\square_H|^{1/d}$ and by noting that the fourth moment of a zero-mean Gaussian random field/variable such as $u - u_{\mathcal{L}}$ is three times its second moment squared. In fact, using Fubini-Tonelli's theorem, we get

$$\mathbb{E}[\|u - u_{\mathcal{L}}\|_{L^4(G)}^4] = \mathbb{E}[\|u - u_{\mathcal{L}}\|^4]_{L^1(G)} = 3 \mathbb{E}[\|u - u_{\mathcal{L}}\|^2]_{L^1(G)}^2, \quad (84)$$

and the rest of the proof in lemma 3.8 of [11] essentially applies. Note that by construction $|\square_H| = 2^{-d\mathcal{L}}$. We can now pull together equations (80), (82) and (83) to obtain,

$$\mathbb{V}[\hat{P}] \leq c \frac{\mathbb{V}[P_{\mathcal{L}}]}{N^q} + \frac{\bar{c}}{N} 2^{-\mu\mathcal{L}}, \quad (85)$$

where

$$\bar{c} = c\tilde{c}|D|^{1/4}\bar{C}(s, D, d) \mathbb{E}[C(\omega)^4]^{1/4} \mathbb{V}[P]^{1/2}. \quad (86)$$

and this concludes the proof. \square

Theorem B.1 states that the statistical error introduced by approximating $\mathbb{E}[P]$ with our hybrid QMC technique can be split in two terms, where the former is the statistical error of a pure randomized QMC estimator and might converge faster than $O(N^{-1/2})$ and the second is a standard MC error correction term that exhibits the usual Monte Carlo rate, but decays geometrically as the Haar level increases. This splitting of the error directly relates to the splitting of white noise as the first term only depends on the truncation $\dot{W}_{\mathcal{L}}$. If $\dot{W}_{\mathcal{L}}$ well approximates \dot{W} , then we expect a pure QMC rate in the pre-asymptotic regime, while if the approximation is poor (small \mathcal{L}), then only a $O(N^{-1/2})$ rate can be expected.

As we see in section 6, even if the asymptotic rate is still $O(N^{-1/2})$, large gains are still obtained in practice in the pre-asymptotic QMC-like regime, especially in a MLQMC setting where not that many samples are needed on the finest levels.